NANOINDENTATION INDUCED THIN FILM FRACTURE

By

KEVIN R. MORASCH

A thesis submitted in partial fulfillment
of the requirements for the degree of

MASTER OF SCIENCE IN MATERIALS SCIENCE AND ENGINEERING

WASHINGTON STATE UNIVERSITY
School of Mechanical and Materials Engineering

MAY 2005

To the Faculty of Washington State University:

The members of the committee appointed to examine the thesis of Kevin R. Morasch find it satisfactory and recommend that it be accepted

_____
(chair)

_____

_____

_____

Acknowledgements

The time and commitment of my advisor Dr. David Bahr for the duration of my research was greatly appreciated. The author would like to thank Sandia National Laboratories and the Department of Energy through the PECASE program under contract DE-AC-04-94AL85000 for the financial support. The author would like to acknowledge Prof. S. Dj. Mesarovic of Washington State University for useful discussions in support of this study and Dr. Jiao and Devon McClain at Portland State University for use and operation of their scanning electron microscope.

NANOINDENTATION INDUCED THIN FILM FRACTURE

Abstract

by Kevin R. Morasch, M.S.
Washington State University
May 2005

Chair: David F. Bahr

Nanoindentation was utilized to induce fracture of brittle thin oxide films on compliant substrates. During the indentation, a load is applied and the penetration depth is continuously measured. A sudden discontinuity, indicative of film fracture, was observed upon the loading portion of the load-depth curve. The mechanical properties of thermally grown oxide films on various substrates were calculated using two different numerical methods. The first method utilized a plate bending approach by modeling the thin film as an axisymmetric circular plate on a compliant foundation. The second method measured the applied energy for fracture. The crack extension force and applied stress intensity at fracture was then determined from the energy measurements.

The plate bending approach estimated the applied radial stress for fracture. The 63 nm thick films were determined to have ultimate strengths between 4.8 and 8.9 GPa. The ultimate stress is a superposition of the bending and membrane stress. A stress intensity at fracture for each of the films was developed by approximating the resulting bending moment and various cracks sizes. At a constant ratio of crack size to oxide thickness of 0.3, the applied stress intensity at fracture of these aluminum oxide films were between 0.46 and 1.20 $MPam^{½}$. The residual stress in the films was assumed to be negligible in the stress intensity calculations.

The energies were calculated from integrating the resulting load-depth curves from indentation. The total energy applied to the system is a superposition of the energy to deform the substrate and the energy to fracture the film. The applied energy to deform the compliant substrate was separated from the energy applied to the film/substrate system resulting in the energy to fracture the film. The energy for fracture was then converted to a crack extension force and a stress intensity using linear elastic fracture mechanics. The crack extension force and stress intensity at fracture for the thermally grown oxide films on aluminum substrates ranged from 0.32 to 1.67 J/m^2 and 0.37 to 0.83 $MPam^{1/2}$, respectively. The titanium oxide had an average crack extension force and stress intensity at fracture of 19.8 J/m^2 and 2.51 $MPam^{1/2}$, respectively.

TABLE OF CONTENTS

Acknowledgements iii

Abstract iv

List of Figures vii

List of Tables ix

Chapter 1 1
Thin film applications 1

Chapter 2 9
Experimental methods and procedures 9
Mechanical properties 9
Nanoindentation 11
Fracture 14

Chapter 3 23
Nano-mechanical Testing for Fracture of Oxide Films 23
Experimental Procedures 25
Results 27
Discussion 41

Chapter 4 54
Energy method to analyze through thickness thin film fracture 54
Experimental Procedure 57
Results 58
Discussion 61

Chapter 5 73
Conclusion and Recommendations 73

LIST OF FIGURES

Figure 2-1 Typcial output data from depth sensing nanoindentation into grade II polycrystalline titanium 12

Figure 3-1 Orientation imaging microscopy of an electropolished 1100 aluminum alloy showing the grain size and crystallographic direction 27

Figure 3-2 Representative load-displacement curves for the 63nm thick oxide on the 99.99% Al substrate with maximum loads prior to and above the discontinuity. 28

Figure 3-3 Micrograph of an indentation made well beyond the first discontinuity with sequential discontinuities in the load-depth curve 30

Figure 3-4 Micrographs of a thermally grown oxide on a mechanically polished 1100Al substrate using atomic force microscopy. Film fracture could not be observed due to the resolution of the atomic force microscope. 32

Figure 3-5 Load-depth results from two indents into an anodized aluminum with maximum loads of 7mN and 10mN along with a resulting load-depth curve into the aluminum substrate without a film. 33

Figure 3-6 Micrographs of indentations on anodized aluminum with maximum loads of a) 10mN and b) 7mN. A circumferential crack occurred around the indentation in micrograph a (10mN max load) where cracking was not present in micrograph b (7mN max load). 34

Figure 3-7 Sequential film cracking of the anodized aluminum..... 35

Figure 3-8. Representative histrogram of the critical loads for the 1100 electropolished substrate with a 54 nm thick film. The histogram shows that critical loads follow a normal distribution. 36

Figure 3-9 The average critical loads were found to be relatively constant for a given substrate. The 99.99% Al substrate had a larger critical load than the 1100 Al substrate. 37

Figure 3-10 Curve fit operations for the mechanically polished 1100 Al substrate 38

Figure 3-11 Loading profile for the indent into the 1100 aluminum substrate reaches a smaller load at a gvien depth than the film substrate system..... 39

Figure 3-12 The total radial stress at fracture for the thermally grown oxide on the 1100Al mechanically polished substrate. The radial stress at fracture increased with film thickness and is dominated by the bending stress. 41

Figure 3-13 Physical observations of circumferential cracking measured a radius of a) 2.3 to 2.5μm and b) 2.9 to 3.7. The fracture radius was estimated to be a) 2.77 and b) 2.82μm using the spherical cavity model. 43

Figure 3-14 Schematic of the applied bending moment for a circular flat plate with clamped edges on a compliant foundation. 44

Figure 3-15 Applied stress intensity factor at fracture in the aluminum oxide – aluminum system assuming a constant normalized crack size of 0.3. 47

Figure 3-16 Applied stress intensity factor at fracture for various a/hf values for the a) 25 nm b) 54 nm and c) 63 nm thick films 49

Figure 4-1 Schematic load depth curves used for fracture energy estimations. The energy estimations for Abdul-Baqi is outlined as OAD, Van der Varst and de With is OAC, and Li et al is ABCD. 56

Figure 4-2 Load-depth results from indentations into grade II polycrystalline Ti with and without an anodized film 60

Figure 4-3 schematic of through thickness cracking of the thin film 61

Figure 4-4 Energy applied to the system during indentation of the anodized titanium 62

Figure 4-5 The energy to fracture the film determined by substracting the energy to deform the substrate from the entire system 63

Figure 4-6 Resulting crack extension forces from 25, 54, and 63 nm thick oxide films on various aluminum substrates 67

Figure 4-7 Resulting stress intensity values at fracture for 25, 54, and 63 nm thick oxide films on various aluminum substrates 68

LIST OF TABLES

Table 3-I Summary of average applied loads and calculated stresses at fracture..... 40

Table 4-I Energy results for thermally grown oxides (TGO) on various aluminum substrates and an anodized titanium 64

Table 4-II Calculated results for crack extension force (G) and stress intensity at frature (K_{app}) for the oxide films grown on various aluminum substrates and an anodized titanium 66

Chapter 1

Thin film applications

There are numerous applications in the world today that utilize thin films for either their mechanical, chemical, or electrical properties. Thin films were first developed with two main objectives. One was to produce capacitors that could obtain a very large capacitance to volume ratio. Smaller capacitors could then be produced with the same amount of charge storage as their larger counterparts. The second purpose was to produce solid state traveling wave devices (semiconductor films). Even though the main objective was to produce smaller electrical devices, these two applications originated the study of thin films and has branched into other fields that we know today. [1] The increasing determination to produce higher quality films with superior properties amplified the study of the film's electrical, mechanical and chemical properties. Thin films could be used for better corrosion resistance, protection against wear, or aesthetics. Hard thin films on soft substrates can be used for knife blades, eye glasses, and car windshields. Thin films have also been shown to improve the lifetime of high speed cutting tools by several hundred percent. [2]

The anodization of aluminum produces a thin oxide layer on the surface by applying a current in an electrolyte bath, oxidating the metal to form an aluminum oxide. Anodizing of aluminum creates an aluminum oxide film that is thicker than the native oxide. There are two different purposes for anodizing aluminum. The first is aesthetics, which is referred to as soft anodizing. The aluminum oxide films during soft anodization contain large pores that can be penetrated with dye. These films do not have very good mechanical properties, but they do enhance corrosion resistance. However, with a slight

change in the production, these films have the ability to have better mechanical properties and have the ability to protect the underlying metal from wear and corrosion.

Thin films are widely used in microelectronics. In some cases they are used a conductor to transmit electricity. [3] Other electrical applications of thin films are thermal insulators, dielectrics, and piezoelectrics. An example of this would be metal-oxide semiconductors (MOS) circuits. MOS circuits utilize multiple film systems for various applications. Thin films are integrated in the active part and during production. During production, thin films are used to mask the surface for particular placement of the next layer and then selectively removed. Piezoelectric devices are widely used in micro electromechanical systems (MEMs). A piezoelectric material can produce current when strained. Since these films are under cyclic loading situations the mechanical response, such as deformation and fracture, need to be addressed to ensure an extensive lifetime.

Magnetic recording hard disk drives use hydrogenerated carbon as a protective and lubricating film for the interface between the head and disk. These carbon films give the head durability and a long lifetime. The main purpose is to prevent tribological damage. Nanoindentation has shown that hydrogenerated carbon films have high hardness values give them optimal mechanical properties. [4]

An Al_2O_3 thin film has been used as an insulator and protection for the production of a special thermocouple. [1] The thermocouple was in an abrasive environment and without the film a small amount of wear would short circuit the thermocouple. Because of its operation, the insulation had to be of high quality both electrically and mechanically.

Another application for thin films is chemical stability and biocompatibility. Thin films are used to protect the underlying materials from corrosive environments, such as the human body and marine environments. The human body contains chemicals that could corrode implant materials when exposed for a prolonged period of time. Titanium alloys have been used as an implant material because of their very stable oxides that form at ambient conditions. [5] Certain implants, hip and knee replacements, are exposed to cyclic loading and an abrasive environment. The thin oxide on the surface has to withstand wear in joints. These materials have to be stable and strong enough to endure the loading situations of everyday life. The mechanical integrity of the passive film has to be determined to prevent premature failure.

Corrosion of metals in marine environments is a large problem. Corrosion costs the United States 279 billion dollars every year in replacement of parts which is about 3.2% of the gross national product. [6] Simple passivating techniques, such as anodizing aluminum, can reduce the corrosion rate. The aluminum oxide film acts as barrier layer between the aluminum and the environment. However, if the film were to fracture the underlying aluminum would be exposed and susceptible to corrosion and wear. Even small scratches in the film that expose the metal would be detrimental. There are other metals, titanium for example, that can be protected by anodization.

One of the most researched materials for thin film applications is diamond. [7] Diamond thin films are very interesting because of their vast applications. Diamonds can be used as thermally conducting layers in electrical devices, they are chemically resistant, and could be doped to produce semiconductivity. Diamonds also have appealing

mechanical properties with a high hardness and strength. The use of diamond thin films may be cheaper to produce and sell than bulk diamonds.

There have been studies on the mechanical properties of thin films, specifically in understanding hardness and the elastic modulus. [8,9] Other researchers have studied friction and wear of thin films. [10-12] Surface topography and the substrate material influence the properties of very thin films. Even under very low loads wear can occur on microparts. [13] Understanding these properties is very important in designing new thin films for various applications. However, understanding the elastic modulus and hardness is not enough. Currently, research has been trying to develop a way to understand thin film fracture. [14-17] Films may have a high hardness and elastic modulus but materials with these properties have low fracture toughness values. Hainsworth *et al* [18] peformed an analysis on the load-depth curves from nanoindentation. It was shown that the loading profile is dependent on the material's hardness and elastic modulus along with the indenter shape. The loading profile can be referred to as a mechanical "fingerprint" for a given indenter shape. Sapphire and copper were determined to have hardness values of 40 and 0.97 GPa and an elastic modulus of 350 and 137 GPa, respectively.

The size in components is reaching the nanometer scale, resulting in the fabrication of nanoelectro-mechanical (NEMs) devices. The mechanical properties of materials change due to the size effect and using bulk properties is not sufficient. The materials are no longer isotropic and smaller defects have a pronounced effect on fracture. A method to characterize thin film fracture at the nanometer scale needs to be developed.

Previously, the only way to test for fracture was to produce free standing thin films and use a technique called bulge testing. The free standing films are usually on the magnitude of microns thick. The testing of freestanding films gives good results but do not take into account the underlying substrate or in some cases multilayer films. Also, producing a free standing thin film with a thickness on the nanometer scale would be difficult.

Chapter 2 will discuss the various methods and procedures that are used to quantify fracture from bulk to thin film applications. A discussion of the different mechanical properties that go along with fracture will be presented. Chapter 2 will discuss details of different bulk and thin film fracture testing methods. It will include descriptions of the Charpy tests, drop weight tear test and how nanoindentation can be used for fracture testing. It will also cover the analytical methods used for quantifying fracture. Quantifying fracture can be done through stating a stress at fracture, the stress intensity ahead of a crack, critical displacements (COD), and determining the energy needed for fracture. Methods in determining fracture of bulk materials are well established for determining fracture toughness. However, a method for determining the fracture toughness of thin films is a current topic of research today.

Chapter 3 will discuss a plate bending approach to quantify thin film fracture. Aluminum oxide films were thermally grown on various aluminum substrates. The films were grown for varying times at the same temperature to produce different thicknesses. Nanoindentation was used to induce thin film fracture. The fracture event can be seen as a depth discontinuity in the loading curve. The surface roughness from the thermally grown films made it difficult to produce micrographs of the fracture. An aluminum

sample was anodized to produce micrographs of the fracture pattern. It will be shown that a circumferential fracture pattern around the indentation occurred. A radial stress and stress intensity at fracture were calculated. In order to determine the radial stress and stress intensity at fracture the films were modeled as an axisymmetric thin plate on a compliant foundation. A discussion will follow about the radial stress at fracture along with a calculation of the bending moment and stress intensity at fracture.

Chapter 4 discusses an energy approach to quantifying thin film fracture. The energy calculation was conducted using the load-depth curves produced during nanoindentation. Thin oxide films were produced on various substrates. Aluminum oxide films were thermally grown on aluminum substrates for varying times and the same temperature to produce different thicknesses. A titanium oxide thin film was anodically grown on a grade II polycrystalline titanium substrate. The energy needed to fracture the film was then normalized to the surface area of the through thickness crack to acquire a crack extension force. An applied stress intensity at fracture was then calculated from the crack extension force using linear elastic fracture mechanics. This will allow a comparison of the plate bending approach to the energy method.

Chapter 5 will be a summary of the current investigation of thin film fracture. The final results from the calculation of the radial stress, stress intensity, and energy at fracture will be given along with a discussion of future work into understanding the mechanical behavior of hard thin films on compliant substrates.

Reference:

[1] L. Johansen, R. Arntzen, S. Bergmann, S. Husa, K.A. Ingebrigtsen, J.S. Johannessen, and J.S. Sandved: Examples of thin film applications in electronic devices, *Thin Solid Films* **50**, 171-185 (1978)

[2] R.F. Bunshah, A.H. Shabiak, R. Nimmagadda, and I. Covy: Machining studies on coated high speed steel tools, *Thin Solid Films* **45**, 453-462 (1977)

[3] V. Le Goascoz: Thin film applications in microelectronics, *NATO Advanced Study Institutes Series, Series B: Physics* **B14**, 417-443 (1976)

[4] N. Ohmae, H. Hara, H. Seki, and I. Endo: Use of the thin solid films at head/magnetic media interface, *Surface Modification Technologies V, Proc. Int. Conf., 5th*, 723-731 (1992)

[5] M.V. Popa, I. Demetrescu, E. Vasilescu, P. Drob, A.S. Lopez, J. Mirza-Rosca, C.Vasilescu, and D. Ionita: Corrosion susceptibility of implant materials Ti-5Al-4V and Ti-6Al-4Fe in artificial extra-cellular fluids, *Electochimica Acta* **49**, 2113-2121 (2004)

[6] Corrosion Costs and Preventive Strategies in the United States**,** Report by CC Technologies Laboratories, Inc. to Federal Highway Administration (FHWA), Office of Infrastructure Research and Development, Report FHWA-RD-01-156, September 2001.

[7] M. Seal: Applications of bulk and thin-film Diamonds, *Materials Science Monographs (Applications of Diamond Films and Related Materials)* **73**, 3-7 (1991)

[8] Zhenghao Gan, Yuebin Zhang, Guoqing Yu, C. M. Tan, S. P. Lau, and B. K. Tay: Intrinsic mechanical properties of diamond-like carbon thin films deposited by filtered cathodic vacuum arc, *J. of App. Phys.* **95,** 3509-3515 (2004)

[9] R. D. Evans, G. L. Doll, P. W. Morrison Jr., J. Bentley, K. L. More, and J. T. Glass: The effects of structure, composition, and chemical bonding on the mechanical properties of Si-aC:H thin films, *Surface and Coatings Technology* **157**, 2-3, 197-206 (2002)

[10] T. Michler, M. Grischke, I. Traus, K. Bewilogua and H. Dimigen: Mechanical properties of DLC films prepared by bipolar pulsed DC PACVD, *Diamond and Related Materials* **7**, 9, 1333-1337 (1998)

[11] V. Prabhakaran and F. E. Talke: Wear and hardness of carbon overcoats on magnetic recording sliders, *Wear* **243**, 18-24 (2000)

[12] E. Sourty, J. L. Sullivan, and M. D. Bijker: Chromium oxide coatings applied to magnetic tape heads for improved wear resistance, *Tribology International* **36** , 389-396 (2003)

[13] H.H. Gatzen and M. Beck: Wear of single crystal silicon as a function of surface roughness, *Wear* **254**, 9, 907-910 (2003)

[14] N.G. Chechenin, J. Bottiger and J.P. Krog: Nanoindentation of amorphous aluminum oxide films II. Critical parameters for the breakthrough and a membrane effect in thin hard films on soft substrates, *Thin Solid Films* **261**, 228-235 (1995)

[15] M. Pang and D.F. Bahr: Thin-film fracture during nanoindentation of a titanium oxide film-titanium system, *J. Mater. Res.* **16**, 2634-2641 (2001)

[16] D.E. Kramer, K.B. Yoder, and W.W. Gerberich: Surface constrained plasticity: oxide rupture and the yield point process, *Phil. Mag. A* **81**, 2033-2058 (2001)

[17] D.F. Bahr, C.L. Woodcock, M. Pang, K.D. Weaver, and N.R. Moody: Indentation induced film fracture in hard film – soft substrate systems, *Inter. J. Frac.* **119/120**, 339-349 (2003)

[18] S.V. Hainsworth, H.W. Chandler, and T.F. Page: Analysis of nanoindentation load-displacement loading curves, *J. Maters. Res.* **11**, 1987-1995 (1996)

Chapter 2

Experimental methods and procedures

This chapter will summarize the important background information on how to analyze thin film fracture. A basic understanding of mechanic properties will first be reviewed. The mechanical properties that will be discussed are elastic modulus, yield strength, and hardness.

These properties can be empirically determined for small volumes using nanoindentation. Well accepted techniques, outlined by Oliver and Pharr [19], will be discussed to determine the elastic modulus, stiffness, and hardness of materials for small volumes.

To understand fracture we will take a look at various tests that are used for bulk materials. This will show what the critical factors that participate in fracture are. A crack can open by three different modes. These different modes of fracture will be reviewed. Finally, this chapter will discuss various methods for quantifying fracture. It will examine a plate bending and an energy approach for fracture. This includes the stress intensity at fracture, crack extension force, and J integral.

Mechanical properties

Mechanical properties are measured values of a material's response to an applied load. The mechanical properties that need to be introduced for the current study are the elastic modulus, yield stress, and hardness. The elastic modulus is a measure of a material's stiffness in the elastic region. It can be measured from a stress-strain curve by the ratio of stress to strain. Mechanical properties of single crystals are not isotropic and

dependent on crystallographic direction. However, certain materials have crystal structures that are highly symmetric. Materials with a face centered cubic or body centered cubic structure have more symmetry than hexagonal close packed. A polycrystalline bulk material with no texturing can be assumed to have isotropic properties. Materials are regularly used in a stress state that is below the criterion for yielding. Yielding is the onset of dislocation nucleation, motion, and multiplication. The Tresca criterion and Von Mises criterion are two numerical methods used to determine the yield stress under uniaxial tension. The Tresca criterion is

$$\tau_{\max} = \frac{\sigma_{p,\max} - \sigma_{p,\min}}{2} \tag{1}$$

where τ_{max} is the maximum shear stress, $\sigma_{p,max}$ is the maximum principle stress and $\sigma_{p,min}$ is the minimum principle stress. The Tresca criterion is also referred to as the maximum shear stress criterion. Von Mises criterion for yielding states that a material will yield when the second invariant of the stress deviator reaches a critical value. The yield stress, σ_0, under uniaxial tension for the Von Mises criterion is

$$\sigma_0 = \frac{1}{\sqrt{2}}\left[(\sigma_1 - \sigma_2)^2 + (\sigma_2 - \sigma_3)^2 + (\sigma_1 - \sigma_3)^2 + 6(\tau_{12}^2 + \tau_{13}^2 + \tau_{23}^2)\right]^{1/2} \tag{2}$$

where σ is the stress normal and τ is the shear stress for a given direction and face on an elemental cube. The subscripts on the stress normal represent the face of the cube and the subscripts on the shear stress represent the face and direction. The orientation and position of the elemental cube in a given material is arbitrary.

Previous studies have tried to understand the yield process for very small volumes. [20-23] The results from these studies showed that materials will elastically load and unload under contact up to a critical load. At a critical load, dislocations would

nucleate and multiply allowing the indenter to plunge into surface. The absence of dislocations prior to yielding was supported from observations made by Syed Asif and Pethica. [22] Further quantification by Bahr *et al* [23] showed that asperities at the surface and pre-existing dislocations could change the stress state ahead of the crack tip and result in a change in magnitude and position of the maximum shear stress. Also, the investigation of the yield stress with the presence of a film or contamination layer showed that the critical load required to cause plastic deformation would increase.

Hardness is a measure of a material's resistance to deformation under an applied contact load. The hardness, *H,* of a material measured through indentation is the applied load, *P*, divided by the projected contact area, A_c, of the indenter.

$$H = \frac{P}{A_c} \tag{3}$$

The elastic modulus and hardness are measurements to give an understanding of how a material will react under different loading situations. However, hardness and elasticity do not consider the onset of fracture. Fracture in a material is dependent on the stress state and shape of the material along with the presence of a defect.

Nanoindentation

Nanoindentation is a common method used to measure the elastic modulus and hardness of small volumes. During the indentation the load and depth are continuously measured as shown in figure 2-1. A diamond indenter tip is used to produce the indentation. Diamond is used to minimize the deformation effect from the tip reducing the deviation of the actual modulus. The theoretical reduced modulus, E_r, can be calculated from the following

$$\frac{1}{E_r} = \frac{\left(1-\nu_1^2\right)}{E_1} + \frac{\left(1-\nu_2^2\right)}{E_2} \tag{4}$$

where E_1 and ν_1 are the elastic modulus and poisson's ratio for the sample and E_2 and ν_2 are the elastic modulus and poisson's ratio for the tip.

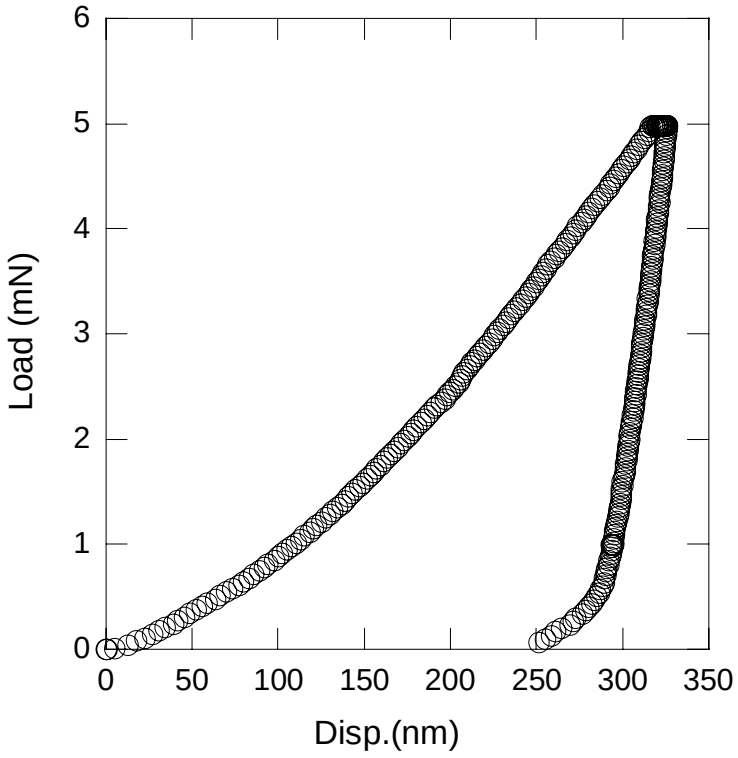

Figure 2-1 Typcial output data from depth sensing nanoindentation into grade II polycrystalline titanium

There are different types of tips commonly used, each of which has a corresponding angle of incidence and sharpness. The different tip shapes used for nanoindentation are a conical tip, the Berkovich tip, spherical, and a cube corner tip. The current research was performed with a cube corner tip. The cube corner tip is the ideal tip for measuring the mechanical properties for small displacements. The lateral deformed area around the cube corner tip is smaller than the Berkovich and conical tips at a given depth. It has an

included angle of incidence of 90° and has a smaller tip radius. The ideal area function $A(\delta)$ for the cube corner tip is

$$A(\delta) = 2.598\delta^2 \tag{5}$$

where δ is the penetration depth. However, the tip deviates from its ideal condition from wear and the area function has to be corrected. The corrected area function can be described by

$$A(\delta) = C_0\delta^2 + C_1\delta + C_2\delta^{1/2} + C_3\delta^{1/4} + C_4\delta^{1/8} + C_5\delta^{1/16} \tag{6}$$

where C_0 through C_5 are correction constants that are empirically determined. The non-idealistic tip does not come to a sharp point. The tip will have some sort of radius to it and can be determined from purely elastic indents into a material with known properties. A curve fit process to the elastic load-depth curves is then performed using Hertzian elastic contact mechanics [24]

$$P = \frac{4}{3}E_r\sqrt{R\delta^3} \tag{7}$$

where P is the applied load and R is tip radius. The stiffness is directly measured from the initial unloading portion of the load-depth curve and the area is calculated from the area function from the tip. The reduced modulus of the sample can be calculated from the resulting load-depth curves given during indentation [19]

$$S = \frac{dP}{dh} = \frac{2}{\sqrt{\pi}}E_r\sqrt{A} \tag{8}$$

where S is the material stiffness and is calculated from the slope of the initial unloading curve and A is the contact area at the maximum load.

Even though nanoindentation is commonly used to measure the elastic modulus and hardness, testing for the fracture toughness and wear can also be performed. Tribology is the study of friction and wear. No matter how smooth a material looks at the macroscopic level it will have surface asperities. The size of these asperities will dictate the frictional forces at the surface. Atomic force microscopy and scratch testing are two methods used to examine the surface topography and wear.

Fracture

There are various testing methods to measure fracture toughness. Tests such as the Charpy test, drop weight test, and Izod test were developed for bulk materials. Each of these tests is able to measure the amount of energy needed to fracture the bulk specimen. The difference between each test is the state of stress that the specimen is in. This limits the ability to compare the numerical results between tests but a direct comparison between materials tested in the same state of stress gives good relative results between different materials or deviation between the same materials. Another way to measure relative toughness is by performing a notched tensile test. This test results in a quantity referred to as the notched sensitivity ratio (NSR). The NSR is a measurement of the stress created from the notched area divided by the ultimate tensile stress from the unnotched area.

Fracture Tests

The most accurately way to perform a fracture test is to produce a triaxial state of stress, $\sigma_x=\sigma_y=\sigma_z=\sigma$. [25] Triaxiality produces brittle fracture and inhibits plastic deformation because shear stresses are omitted. With the lack of shear stresses in the

material the total energy for fracture will be to separate two atomic planes and cause brittle fracture. There are other techniques used to produce brittle fracture. For example, a very high strain rate can produce brittle fracture.

The Charpy V notch test [26] uses high speeds and impact to produce brittle fracture. A sample with a prescribed notch size is mounted at the base of the machine and a hammer with 240 ft-lb of energy strikes the sample. An absorbed energy measurement is then made to determine the fracture energy. A similar test is the drop weight tear test. [27] The drop weight tear test was invented to test large flat plates with welded regions where the weld acts as the starting defect. The problem with these tests is that complete brittle fracture does not occur. These tests will give energy to fracture for the test performed but can not be used in comparison with other fracture tests.

A typical indentation test to determine the fracture toughness of bulk ceramic materials is micro-indentation. Vickers hardness tests use a diamond indenter in the form of a right pyramid with a square base and an angle of 136 degrees between opposite faces. The load is applied and held for 10 seconds. The load is then removed and the length of the cracks from the corners of the indent is measured. [28] A study by Evans and Charles [29] measured the fracture toughness using indentation. The fracture toughness was a function of hardness, Poisson's ratio, coefficient of friction, and two empirically determined coefficients. It was interesting to note that the ratio of crack length to plastic zone size is larger for soft materials than hard materials. Keer *et al* [30] analyzed Vickers indentation as three dimensional fracture. The plastic zone was modeled as one half of a prolate spheroid and the induced cracks were one half penny shaped crack. The crack opening displacement, plastic strain in the crack, and the plastic

stress field were determined. The integration is a function from direct measurements of the crack length, plastic zone size, and the applied load.

Nanoindentation can measure the mechanical response of materials, for example elastic-plastic properties, creep, viscoelasticity, and fracture. Nanoindentation can be used for fracture testing similar to macroindentation. A load is applied which will induce cracking in a brittle material. [31] Nanoindentation units have depth sensing capabilities that will produce a load-depth curve. This curve gives insight into the amount of energy applied to a system.

Modes of Fracture

Stresses in cracked bodies can lead to three different modes the opening a crack. [32] Mode I is considered the “opening mode” where normal stresses force the crack apart. The displacement of the crack faces are perpendicular the plane of the crack. Mode II is considered the “sliding mode”. This is caused from in plane shearing forces where the crack displacement is in the plane of the crack and perpendicular to the leading edge. Mode III or “tearing mode” is caused from out of plane shear stresses and the crack displacement is in the plane of the crack and perpendicular the leading crack tip. One or all three of the modes could be present during fracture. Mode III situations are usually the worst case scenarios for fracture. However, in the current study of thin film fracture, mode I is dominant.

Quantitative analysis

There are different analytical methods to quantify fracture. One method is to determine the stress at fracture. However, using stress as a fracture criterion has its

problems. Stress is not a material property and is dependent on the dimensions of the specimen. Different states of stress will produce different mechanisms for fracture. A situation of plane stress occurs when there is no constraint in the thickness and $\sigma_3 = 0$ and all other in plane stresses are not zero. Plane strain situations occur when $\varepsilon_3 = 0$ and all of the plane strains are not equal to zero. A state of plane stress creates a larger plastic zone ahead of the crack tip than plane strain. In most cases, the state of stress is a mixture of these two situations.

Another way of looking at fracture is displacement. Crack opening displacement (COD) is defined that when the faces of the crack reach a critical distance propagation will occur to reduce the elastic strain energy around the crack. COD is a solution for linear elastic fracture mechanics. The critical displacement is dependent on the applied stress and the elastic modulus. A correction for plastic deformation ahead of the crack may be applied due to blunting of crack tip radius. This correction leads to crack tip opening displacement (CTOD). Correction for the plastic deformation ahead of the crack tip yields that CTOD is dependent on the material's yield stress and the stress intensity. [32]

The stress state ahead of a crack tip is different than the gross applied stress. The stress state is described by a set of field equations as a function of the factor K in polar coordinates. The factor K, known as the stress intensity factor, is determined by the loading situation, dimensions of the body and defect shape and size. The general solution for an infinite plate under tension with a central crack is [32]

$$K = \sigma\sqrt{\pi a} \tag{9}$$

where σ is gross applied stress and *a* is half the crack length. This equation can be modified to take into account a small amount of plasticity (ductile materials, where plasticity can not be ignored, use the J-integral approach), the shape of the crack, and position of the crack. Another variable that can be taken into account to modify the stress intensity equation is size of the crack in comparison to the cracked body. Using the stress intensity factor as a fracture criterion assumes that linear elastic fracture mechanics (LEFM) is used. LEFM can only be used if the plastic deformation ahead of the crack front is small. This is usually the case when the macroscopically applied stress is smaller than 80% of the yield stress. If the plastic zone ahead of the crack tip is extensive the J integral fracture criterion has to be used.

Another way to quantify fracture is by measuring the amount of energy needed for fracture. A brief description of fracture is the separation of two adjacent planes of atoms. It takes a certain amount of energy for separation. This energy comes from breaking the atomic bonds, deformation of the material prior to crack propagation, and a small amount may go into heat. The crack extension force and the J integral are two methods that utilize energy as a fracture criterion.

An energy method to linear elastic fracture mechanics is the use of the critical crack extension force G. This can be used when the plastic zone ahead of the crack front is small. This typically is the case with materials that have low toughness values. Materials with low toughness values typically have high strengths. The general form for the crack extension force is

$$G = \left[\frac{P * d\Delta - dU}{dA} \right] \tag{10}$$

where P is the applied load, $d\Delta$ is the change in displacement, dU is the change in elastic strain energy, and dA is the new surface produced from crack propagation. A specific form of the crack extension force exists when the load is held constant.

$$G = \left(\frac{dU}{dA} \right)_{p=cons\tan t} \tag{11}$$

Cheng *et al* [33] showed that the total work applied by indentation could be calculated by integrating the loading curve to the maximum depth. It was shown that the total work is a superposition of reversible and irreversible work. The strain energy term for the crack extension force can be determined through depth sensing indentation by integrating the resulting load-depth curve to the critical depth at fracture.

$$U = \int_0^{\delta_c} P(\delta) d\delta \tag{12}$$

where P is the loading profile and $d\delta$ is the range of integration.

The J integral is based on energy conservation and was developed for low strength ductile materials. The J integral will reach a critical value when fracture occurs, similar to the crack extension force and stress intensity factor. It was shown by Rice that a line integral around a crack would solve a 2 dimensional crack problem and is path independent. [34]

$$J = \int_\Gamma \left(W dy - T \frac{du}{dx} ds \right) \tag{13}$$

where W is the strain energy per unit volume, Γ is the enclosed path around the crack front, T is the outward traction vector acting on the enclosed path, du is the change in displacement, ds is an increment on the enclosed path, and x and y are rectangular coordinates. The J integral is very close to the calculation of the crack extension force for

brittle materials under constant load. In the case of linear elastic fracture mechanics the J integral is equivalent to the crack extension force, G [32]

$$J = G = \frac{K^2}{E} \tag{14}$$

where K is the stress intensity and E is the plane strain elastic modulus.

Ceramic materials typically have a high elastic modulus and hardness. These properties make them very important but typically fracture catastrophically with small amounts of plastic deformation. An assumption that will be made to simplify calculations in this study is that the film will only elastically deform prior to fracture allowing linear elastic fracture mechanics to be utilized for analysis.

Reference:

[19] W.C. Oliver and G.M. Pharr: An improved technique for determining hardness and elastic modulus using load and displacement sensing indentation experiments, *J. Mater. Res.* **7**, 1564-1583 (1992)

[20] D.E. Kramer, K.B. Yoder, and W.W. Gerberich: Surface constrained plasticity: oxide rupture and the yield point process, *Phil. Mag. A* **81**, 2033-2058 (2001)

[21] N. Gane and F.P. Bowden: Microdeformation of solids, *J. Appl. Phys*. **39**, 1432-1435 (1968)

[22] S.A. Syed Asif and J.B Pethica: Nanoindentation creep of single-crystal tungsten and gallium arsenide, *Phil. Mag. A* **76**, 1105-1118 (1997)

[23] D.F. Bahr, D.E. Kramer, and W.W. Gerberich: Non-linear deformation mechanisms during nanoindentation, *Acta Mater.* **46**, 3605-3617 (1998)

[24] K.L. Johnson: *Contact Mechanics*, (Cambridge University Press, Cambridge, U.K., (1985)

[25] G. Dieter: *Mechanical Metallurgy third edition*, McGraw-Hill Book Company, New York, New York, U.S.A (1986)

[26] ASTM E23-02a Standard test methods for notched bar impact testing of metallic materials, *ASTM Book of Standards* Vol. 03.01 (2004)

[27] ASTM E208-95a Standard test method for conducting drop-weight test to determine nil-ductility transition temperature of ferritic steels, *ASTM Book of Standards* Vol. 03.01 (2004)

[28] B.R. Lawn and T.R. Wilshaw: Indentation Fracture: Principles and Applications, *J. Mater. Sci.* **10** 1049-1081 (1975)

[29] A.G. Evans and E.A. Charles: Fracture toughness determinations by indentation, *J. Am. Ceram. Soc.* **59**, 371-372 (1976)

[30] L.M. Keer, T.N. Farris, and J.C. Lee: Knoop and Vickers indentation in ceramics analyzed as a three-dimensional fracture, *J. Am. Ceram. Soc*. **69**, 392-396 (1986)

[31] D.J. Morris, S.B. Myers, and R.F. Cook: Sharp probes of varying acuity: Instrumented indentation and fracture behavior, *J. Mater. Res*. **19**, 165-175 (2004)

[32] D. Broek: *Elementary engineering fracture mechanics fourth edition*, Kluwer Academic Publishers, Dordrecht (1986)

[33] Y.T. Cheng and C.M. Cheng: Scaling, dimensional analysis, and indentation measurements, *Mater. Sci. and Eng. R* **44**, 91-149 (2004)

[34] J.R. Rice: A path independent integral and the approximate analysis of strain concentration by notches and cracks, *J. Appl. Mech.* **35**, 379-386 (1968)

Chapter 3

Nano-mechanical Testing for Fracture of Oxide Films

Metals, such as aluminum and titanium, form native oxides on the surface. In turn, these oxides enhance protection of the underlying metal against wear and corrosion. The mechanical integrity of these protective oxides needs to be characterized in order to increase protection against harsh environments. Improving the mechanical properties will lead to better product quality and a longer lifetime.

Nanoindentation has been used to study the mechanical response of various metal/ oxide systems. [35,36] During the loading of these systems, a sudden discontinuity has been observed. In some cases the sudden discontinuity has been attributed to yielding and nucleation of dislocations in the substrate [37,38] and other cases have shown that it was caused by film fracture. [35,36,39-41] Previous studies have demonstrated via atomic force microscopy, electron microscopy, or optical microscopy that a film fracture event generates a circumferential crack around the indentation in the oxide film. [36,42,43]

Chechinen and co-workers studied the critical load and depth of the discontinuity during indentation for an Al_2O_3/Al system as a function of film thickness. [35] They showed that both the critical load and depth for thicker films followed a Weibull type distribution with parameters typical to materials with moderate brittleness and hardness. A model was developed to describe the critical parameters for load and depth. The model was in good agreement for thicker films but some deviation occurred for thinner films.

Another way to quantify film fracture is to determine the radial stress as a function of contact load needed for failure. Various analytical methods have been used to model the system. [44,45] One method was to model the film as an axisymmetric circular

plate with clamped edges supported on a compliant foundation. [36,40,41] Pang and Bahr used nanoindentation to test an anodically grown TiO_2 film on a mechanically polished Ti substrate. [36] This system exhibited plastic deformation prior to the load at which the discontinuity was seen which indicates that the discontinuity was owing to thin film fracture Using the axisymmetric clamped plate model, a critical stress was quantified for each film thickness by using a superposition of the bending stress and membrane stress induced by the contact load. Stress is a common way to measure the mechanical response of materials. However, the stress at failure is influenced by the film thickness and defect density and is not truly a material property.

A study by Weppleman and Swain used micro-indentation to study thin film fracture. [46] TiN films of various thicknesses were grown on stainless steel by physical vapor deposition methods. The induced stresses in the film/substrate system were determined by using finite element analysis. It was found that for films which are thin (h_f) compared to the radius (R) of the indenter tip (R/h_f >6.7) the first fracture was caused by high radial stresses outside the contact radius. A study by Chai and Lawn showed that the highest radial stress at the surface occurred in the region outside the contact edge for thin films. [47] Thicker films were found to have a maximum radial stress near the edge of the contact radius. A weight function was used to plot the stress intensity factors K_I and K_{II} against a/h_f where a is the crack size and h_f is the film thickness. The thin film fracture was dominated by a Mode I loading situation.

In this current study a first order analytical model was developed to quantify thin film fracture using nanoindentation. Aluminum oxide films of various thicknesses were thermally grown on aluminum substrates. A first order approximation of the stress

intensity at fracture was developed assuming that the critical flaw was a penny shaped surface crack which encircles the region of contact, similar to that observed in previous studies. [36,42,43] The crack size was chosen to not exceed 30% of the film thickness. The stress intensity at fracture was estimated using the overall bending moment. The radial force was neglected because the film deflection was small compared to the film thickness. Chechenin *et al* calculated the stress intensity factor using the membrane stress because film deflections were larger compared to the film thickness. [35]

Experimental Procedures

Two different aluminum substrates were used in this study. The samples were made from a commercially available ingot of 1100 aluminum and a 99.99% pure Al ingot. The substrates were encapsulated in an evacuated quartz tube, back filled with argon gas and annealed at 500°C for 24 hrs.

After annealing, samples from both materials were polished. One set of samples from the 1100 Al and 99.99% pure aluminum were mechanically polished by grinding the samples to 1200 grit and then polishing to 0.05μm with colloidal silica. Another set of samples from the 1100 Al was electropolished in an electrolyte of 25% Nitric acid and 75% methanol at -20°C using a bias of 10V. After polishing, different film thicknesses were obtained by thermally growing oxides at 500°C for 1, 2, and 3 hrs and air quenching at room temperature. The oxide growth was shown by Aylmore, Gregg, and Jepson to follow a linear law with time between 500 and 550°C. [48] Using the linear law, the theoretical film thickness should be 35nm, 50 and 65 nm for 1, 2, and 3 hrs growth time at 500°C, respectively. The oxide thicknesses were measured using a Gaertner spectral

ellipsometer, and were determined to be 25, 54, and 63 nm for 1, 2, and 3hr growth times, respectively. The oxide thickness was not influenced by the underlying substrate in these materials. Gulbransen and Wysong studied the growth of aluminum oxide on aluminum and over a temperature range of 400 to 500°C. [49] The oxide layer was found to be amorphous in structure but the heating time was only 30 min. [49,50]

Nanoindentation was carried out using a Hysitron Triboscope coupled with a Park Autoprobe scanning probe microscope. The indentations were made with a cube corner diamond indenter (90° included angle) with an effective tip radius of 570 nm. The tip radius was calculated by performing a series of elastic loading curves in tungsten. A tip radius was then calculated for each elastic curve using the Hertzian elastic loading profile. [51]

The aluminum substrates were polycrystalline. Three grains with different crystallographic orientations on the 99.99% pure aluminum substrate were tested using nanoindentation to examine influence of grain orientation. The orientations were determined using electron beam scattering diffraction (EBSD). EBSD is performed with the used of a scanning electron microscope (SEM). The electron beam from the SEM strikes the sample and travels beneath the surface. The crystallographic planes cause electron diffraction and a distinct pattern of bands are made on a phosphor screen. The pattern is referred to as Kikuchi bands and are distinct for a given crystal structure. An EBSD image of one of the samples can be seen in figure 3-1 along with the orientation color code for a face centered cubic crystal structure. The tested areas on the three different are represented as squares in figure 3-1. The resulting load-depth curves from each graph overlap each other. This shows that the surface of the sample is more

influential to the loading profile than the orientation and therefore will not be considered in this study.

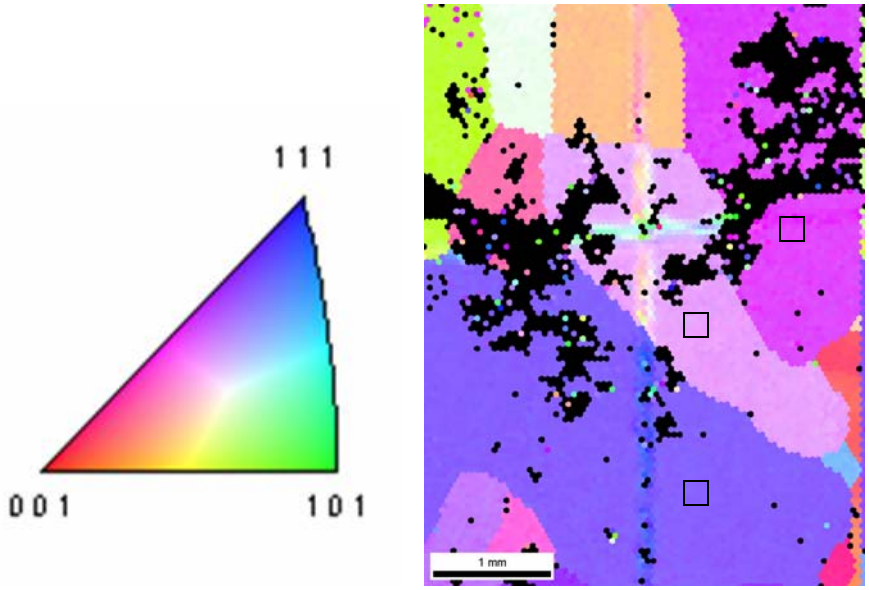

Figure 3-1 Orientation imaging microscopy of an electropolished 1100 aluminum alloy showing the grain size and crystallographic direction

The Al_2O_3/Al systems were then indented with maximum loads ranging from 15μN to 500μN. A minimum of 10 indents were randomly positioned with a maximum load of 50 μN for each film thickness. The loading time to the maximum load was held constant at 10 seconds for each indent, and the critical loads and depths at the first excursion were recorded. Atomic force microscopy (a Park Autoprobe CP) was used to measure surface roughness.

Results

Two typical load depth curves from indentations into the electropolished 1100 aluminum with a 63 nm thick oxide are shown in figure 3-2. A maximum load for one of the indentations was chosen to produce a discontinuity in the load-depth curve. The

second indent was unloaded prior to the load at which the discontinuity occurred in the other indentation.

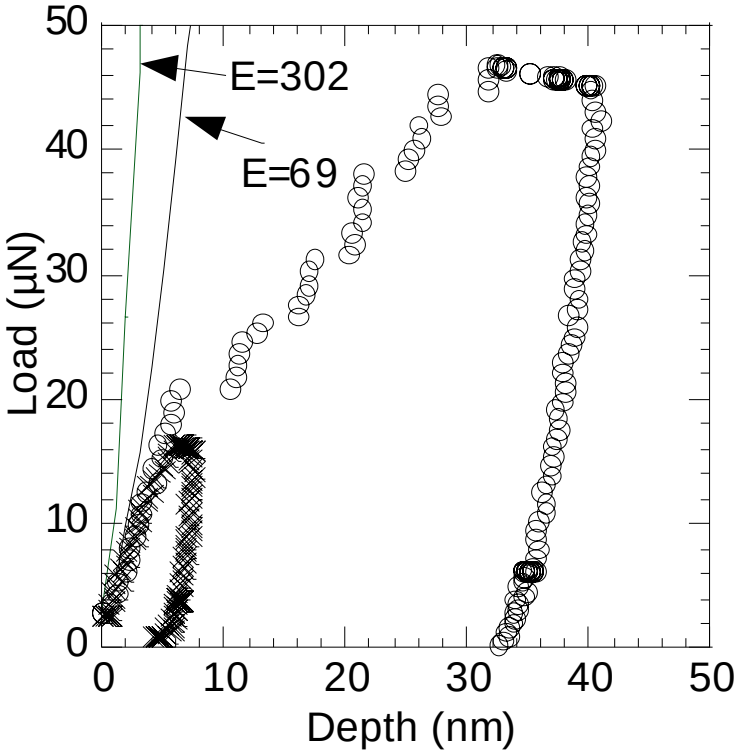

Figure 3-2 Representative load-displacement curves for the 63nm thick oxide on the 99.99% Al substrate with maximum loads prior to and above the discontinuity.

The load-depth curve with a maximum load prior to the discontinuity resulted in a residual depth after indentation. This residual depth demonstrates that plastic deformation occurred in the system during indentation, indicating the presence of dislocations and the discontinuity was not caused from a yielding phenomenon (a sudden nucleation and multiplication of dislocations). The two solid lines represent the theoretical elastic response if the indentations followed the Hertzian elastic response for aluminum (E_r= 69 GPa) and crystalline aluminum oxide (E_r = 302 GPa) for the tip. The indentation experiment shows that there is a deviation from the theoretical elastic response, again

suggesting plastic deformation is occurring in these systems prior to the discontinuity. This therefore precludes dislocation nucleation as the cause of the discontinuity and suggests it is due to film fracture. [36] Similar curves were produced for the mechanically polished 1100 aluminum and mechanically polished 99.99% pure aluminum.

The cause of the sequential discontinuities after the first could not be determined. Multiple discontinuities have also been attributed to the phenomenon of yielding. This is referred to as “staircase” yielding. During indentation mobile dislocations may become immovable through interactions with diffusing solute atoms or other dislocations. [52] The immovable dislocations would break free and become mobile at a critical stress. Continuous interaction of dislocations and increasing the indentation load could lead to “staircase” yielding. However, in the current experiment it would be unlikely that dislocation nucleation would become the controlling factor during this indent. Observations show that multiple cracking and crushing of the film is occurring during continuous loading past the first discontinuity. Figure 3-3 shows an indentation with a maximum load well beyond the critical load for the first excursion.

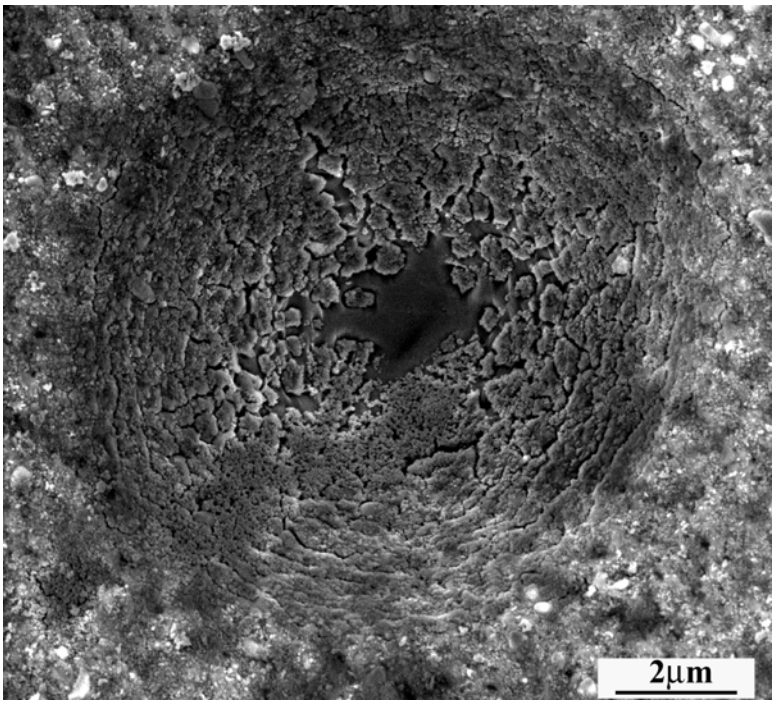

Figure 3-3 Micrograph of an indentation made well beyond the first discontinuity with sequential discontinuities in the load-depth curve

Circumferential cracking dominates at the edge of the indentation. Crushing of the film occurs as closer to the center of the indentation. The center region is exposed aluminum.

Atomic force microscopy was carried out to attempt to identify the crack around the indentation, which was expected to be similar to previous studies. [36,42,43] However, the roughness of the thermally grown oxide was approximately 20-30% of the film thickness. An AFM image of the thermally grown oxide films can be seen in Figure 3-4. He, Evans, and Hutchinson [53] has also been shown that a ratcheting effect occurs on thermally grown hard films on ductile substrates. The ratcheting effect is caused from the film undergoing compression during the cooling of the film from thermal expansion. The ductile substrate alloyed the film to deform and a rough surface is produced. Tolpygo and D.R. Clarke [54] studied the growth of an alumina thin film by thermal oxidation on

an Fe-Cr-Al alloy. The study was found to show a wrinkling morphology of the alumina surface. This provided a rough surface which limited the ability to find cracks in the oxide during indentation. This rough surface, which exhibited equiaxed grains of approximately 100 nm in diameter, made unambiguous identification of the specific crack of interest impossible. However, this roughness provides the motivation for choosing a possible initial crack size in the following fracture analysis. Both AFM and use of the Hysitron imaging system show no evidence of any significant pile up or sink in phenomena in the materials in this study.

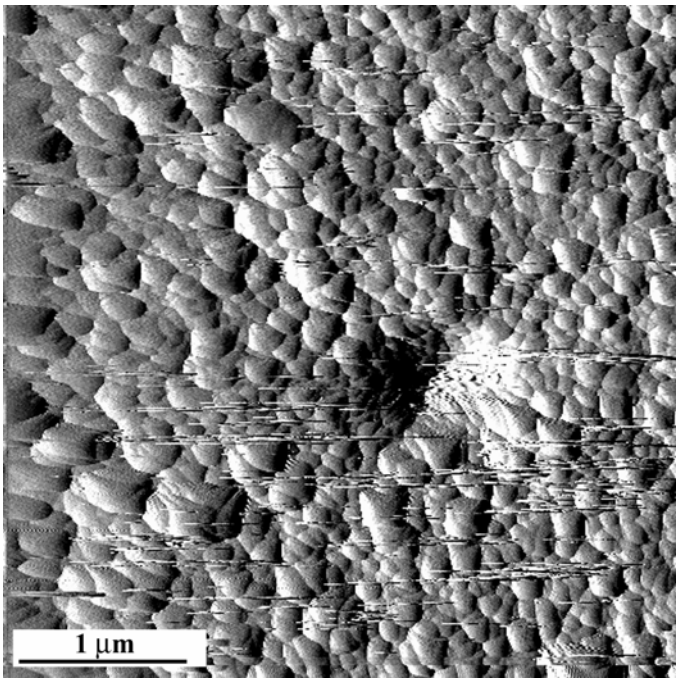

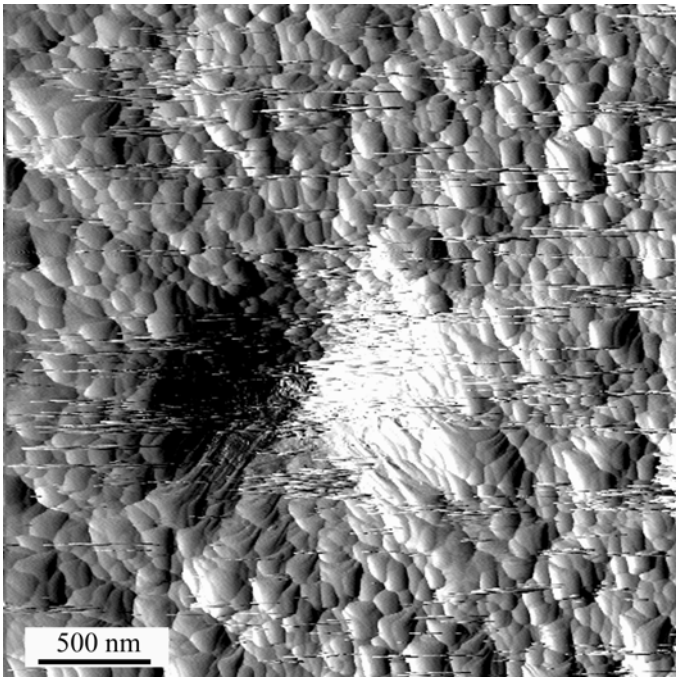

Figure 3-4 Micrographs of a thermally grown oxide on a mechanically polished 1100Al substrate using atomic force microscopy. Film fracture could not be observed due to the resolution of the atomic force microscope.

A scaled up version of the aluminum oxide-aluminum system was produced by anodization. Producing the oxide by means of anodization was chosen because of its minimal surface roughness. The anodized film contained porosity but the porosity did not effect the position of the circumferential crack and was thicker than the thermally grown oxides. This was to increase the resolution in order to observe the cracking in the film. Figure 3-5 shows the corresponding load-depth curves for the indentation micrographs in figure 3-6. The load-depth curve that reached a maximum load of 10mN produced circumferential cracking around the indentation (fig. 3-6a). The crack was positioned outside the contact area of the indenter tip. The tip contact radius is noted as a_c and the crack distance from the center of the indent is marked as c. Figure 3-6b shows the corresponding micrograph for the load-depth curve with a maximum load of 7mN. The corresponding load-depth curves for the shows that the circumferential is accompanied

by a discontinuity at about 8mN. The discontinuity at 5mN was caused from the porosity in the film. The porosity allowed the film to be crushed under the applied load of the indenter. This does not occur in the thermally grown oxides because porosity was likely not present.

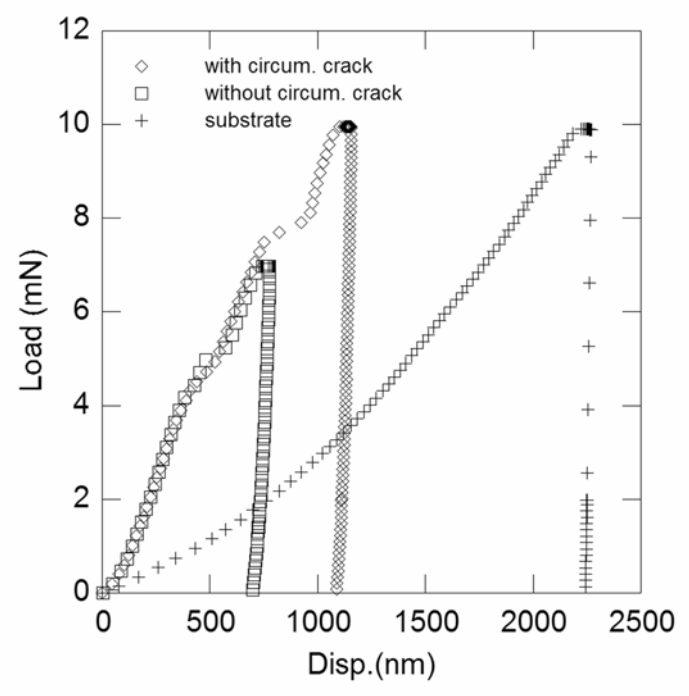

Figure 3-5 Load-depth results from two indents into an anodized aluminum with maximum loads of 7mN and 10mN along with a resulting load-depth curve into the aluminum substrate without a film.

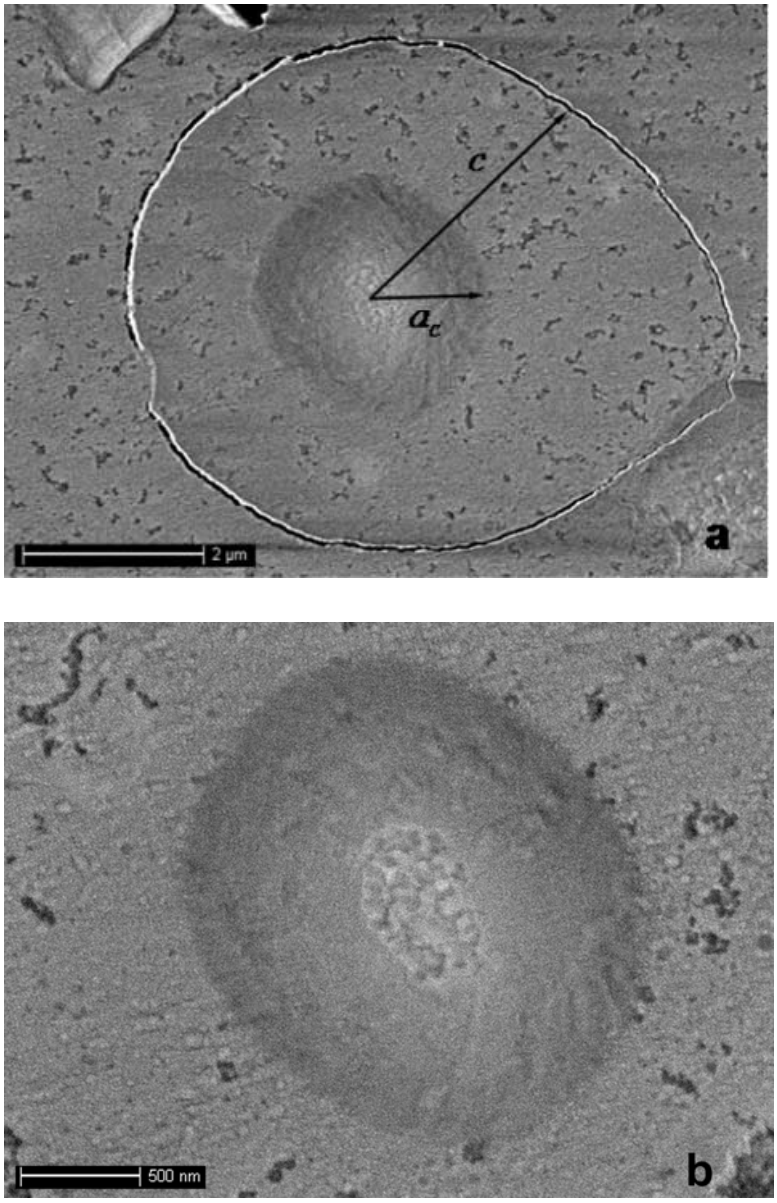

Figure 3-6 Micrographs of indentations on anodized aluminum with maximum loads of a) 10mN and b) 7mN. A circumferential crack occurred around the indentation in micrograph a (10mN max load) where cracking was not present in micrograph b (7mN max load).

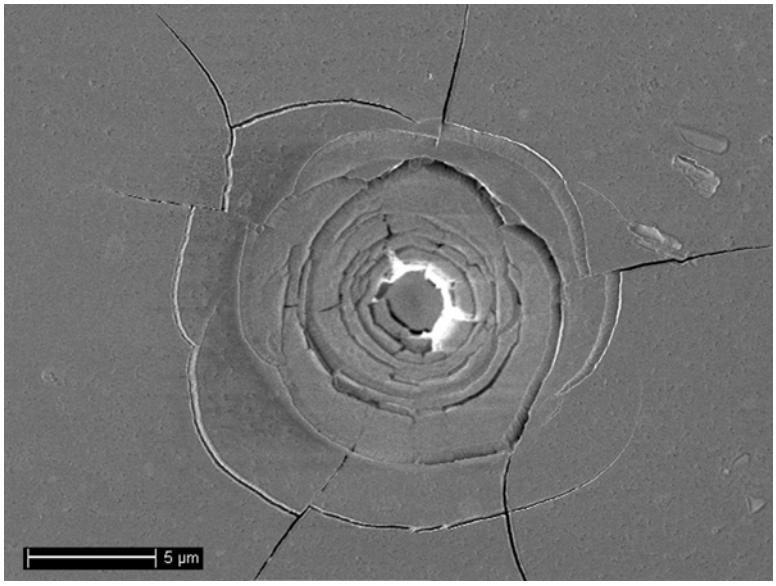

Figure 3-7 Sequential film cracking of the anodized aluminum

Figure 3-7 shows an indentation beyond the first the first discontinuity for the anodized aluminum. The indentation beyond the first discontinuity showed that sequential circumferential cracking occurred and then radial cracks developed, very similar to figure 3-3. The sequential circumferential cracks were present in an indentation study of submicron silica films on a polymer substrate by Andersson *et al*. [43] The silica film had an amorphous structure similar to the films in the current study.

The critical load and depth at each discontinuity were recorded and a histogram was produced for each substrate as shown in figure 3-8. The first critical loads and depths were found to follow a normal distribution.

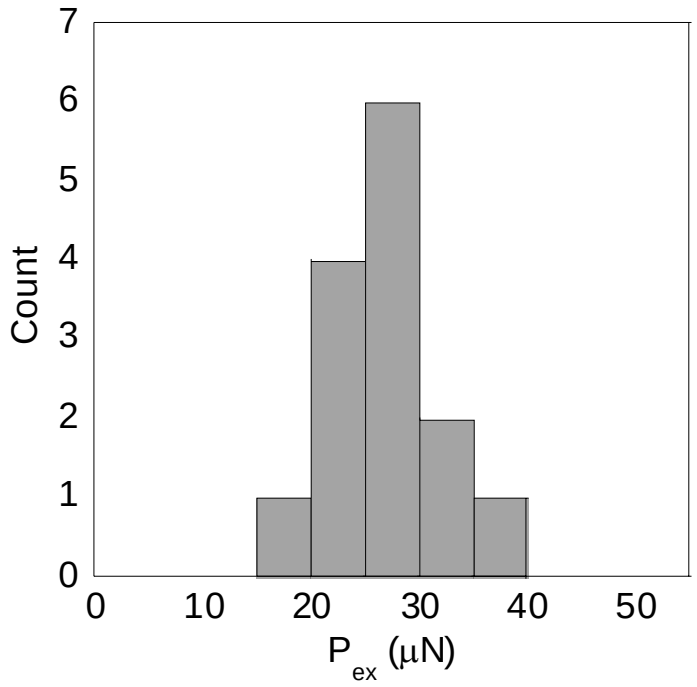

Figure 3-8. Representative histrogram of the critical loads for the 1100 electropolished substrate with a 54 nm thick film. The histogram shows that critical loads follow a normal distribution.

A summary of the average critical loads for the oxides grown on the 1100 and 99.99% mechanically polished substrates along with the 1100 electropolished aluminum substrate is shown in figure 3-9. The applied load at fracture stayed constant for each substrate with increasing film thickness. The thermally grown oxide on the 99.99% pure aluminum substrate was found to fracture at critical loads larger than the oxide grown on the 1100 aluminum substrates. The 25 nm thick film on the 99.99% aluminum substrate fractured at an average load of 49.4 μN. The 25 nm thick oxides on the mechanically polished 1100 and the electropolished 1100 substrates fractured at an average load of 29.26 and 24.75 μN, respectively.

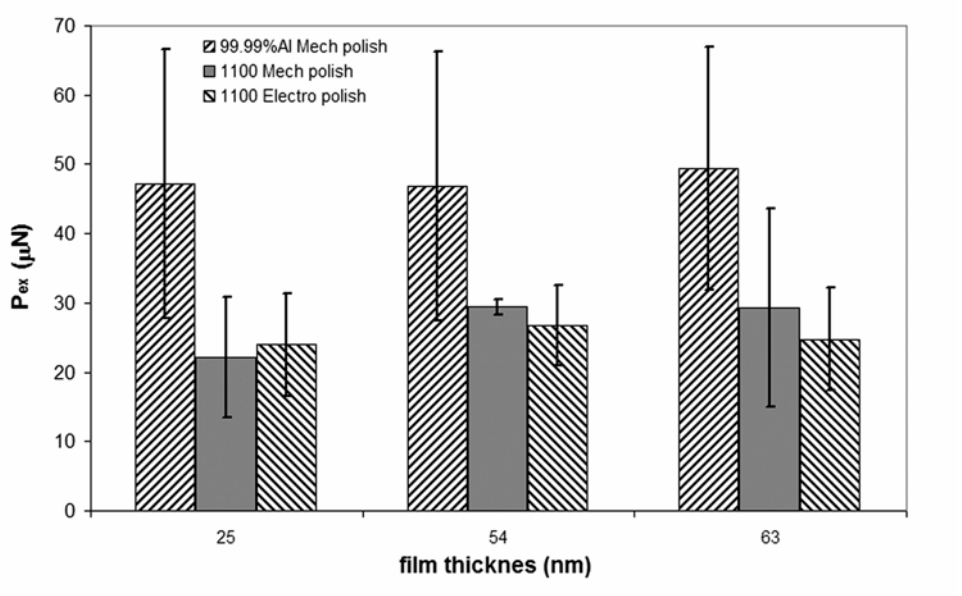

Figure 3-9 The average critical loads were found to be relatively constant for a given substrate. The 99.99% Al substrate had a larger critical load than the 1100 Al substrate.

Estimating the applied radial stress at failure is a better way to evaluate thin film fracture than merely examining the loads if we are going to compare results between laboratories. The radial tensile stress applied to the film is a function of film thickness, plastic zone size in the substrate, modulus of the film, and the critical deflection of the film. The radial stress at failure was determined by modeling the indentation as a point load on a hard elastic plate on a soft substrate in similar tests during previous studies. [36,41] During indentation it is assumed that the film elastically deforms until brittle fracture. We assume that given the relative hardness differences between alumina and aluminum that the plastic deformation in the system is occurring entirely in the substrate. The film can then be modeled as an elastically deforming axisymmetric circular plate with a clamped edge. The clamped edge was defined as the end of the substrate plastic zone radius. The plastic zone radius can be approximated by [55]

$$c = \sqrt{\frac{3P_s}{2\pi\sigma_f}} \tag{15}$$

where P_s is the load carried by the substrate and σ_f is flow stress. The load carried by the substrate was found to empirically follow a power law relationship from the load (P) displacement (δ) curve of the substrate with just the native oxide. [56]

$$P_s = K\delta^n + C \tag{16}$$

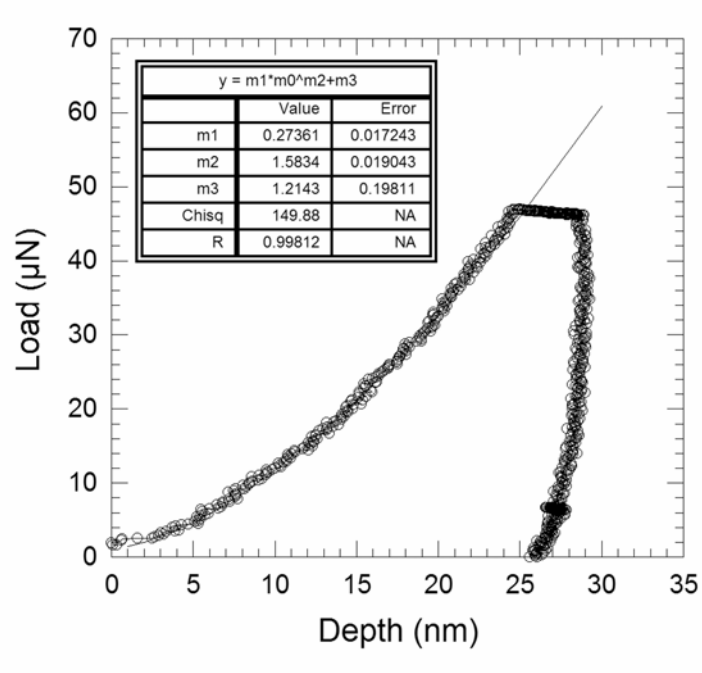

Figure 3-10 Curve fit operations for the mechanically polished 1100 Al substrate

The constants for the mechanically polished 1100 substrate were 0.274, 1.58, and 1.21 for K, n, and C, respectively. The constants were taken from curve fitting the loading profile from indentations with a maximum load of 900μN. Figure 3-10 illustrates the curve fit on an indent with a maximum load of 50 μN. Superimposing the loading profile of the substrate and the load-depth curves from the film/substrate system shows that the at a given depth the substrate will carry a smaller load. The load-depth curves from the

underlying substrate and the film/substrate system can be seen in figure 3-11. The oxide film has a higher stiffness than (E = 411GPa) than the underlying substrate (E=72 GPa) which ables the film/substrate to carry a higher load at lower depths than solely the substrate.

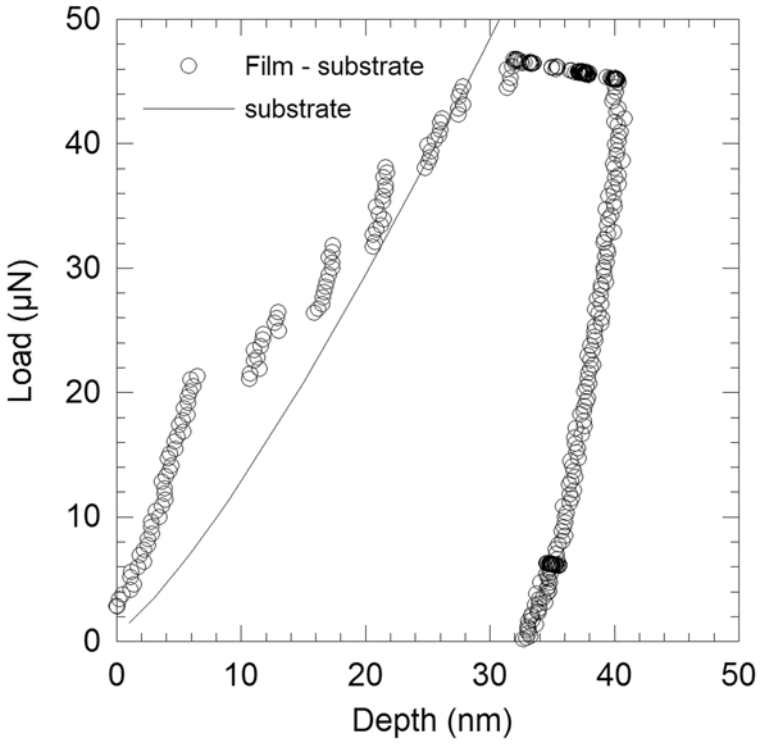

Figure 3-11 Loading profile for the indent into the 1100 aluminum substrate reaches a smaller load at a gvien depth than the film substrate system

The radial stress has been demonstrated to cause the through thickness cracking of a hard film on soft substrate. [46] The radial stress prior to fracture can be estimated from a superposition of the bending stress and stretching stress created from the contact load [57]

$$\sigma_r = 0.357E_f \frac{\delta^2}{c^2} + 2.198E_f \frac{\delta h_f}{c^2} \quad (17)$$

where δ is the depth at fracture, h_f is the film thickness, E_f is the modulus of the film (assumed to be 411 GPa, references provide ranges between 380 [58] and 415 [59] GPa) and 0.375 and 2.198 are empirical constants for the stretching and bending stresses. [57] The bending stress, stretching stress, and the overall radial stresses at fracture for the chosen parameters can be seen in table 3-I.

Table 3-I Summary of average applied loads and calculated stresses at fracture

Substrate	h_f (nm)	Load (μN)	bending stress (GPa)	membrane stress (GPa)	radial stress (GPa)
99.99% Mechanically polished	25	47.23 +- 19.40	2.44 +- 0.15	0.15 +- 0.10	2.59 +- 0.10
	54	46.81 +- 19.37	5.28 +- 0.24	0.19 +- 0.07	5.57 +- 0.18
	63	49.40 +- 17.53	6.02 +- 0.33	0.19 +- 0.09	6.21 +- 0.29
1100 Mechanically polished	25	22.12 +- 8.71	3.47+- 0.04	0.14 +- 0.01	3.61 +- 0.03
	54	29.43 +- 1.14	7.43 +- 0.09	0.15 +- 0.01	7.58 +- 0.08
	63	29.26 +- 14.35	8.73 +- 0.24	0.14 +- 0.03	8.87 +- 0.21
1100 Electropolished	25	23.97 +- 7.43	1.86 +- 0.06	0.10 +- 0.02	1.96 +- 0.04
	54	26.73 +- 5.85	3.92 +- 0.19	0.11 +- 0.03	4.03 +- 0.02
	63	24.75 +- 7.38	4.68 +- 0.22	0.10 +- 0.04	4.77 +- 0.19

The film thickness and the radial stress to failure were linearly proportional as the thickness was increased from 25 nm to 63 nm. As mentioned before, the radial stress is a superposition of a bending stress along with membrane stress. Separating the total radial stress at failure shows that the bending stress is significantly larger than the membrane stress in this film system. The separation of the total radial stress at fracture into its bending stress and membrane stress can be seen figure 3-12.

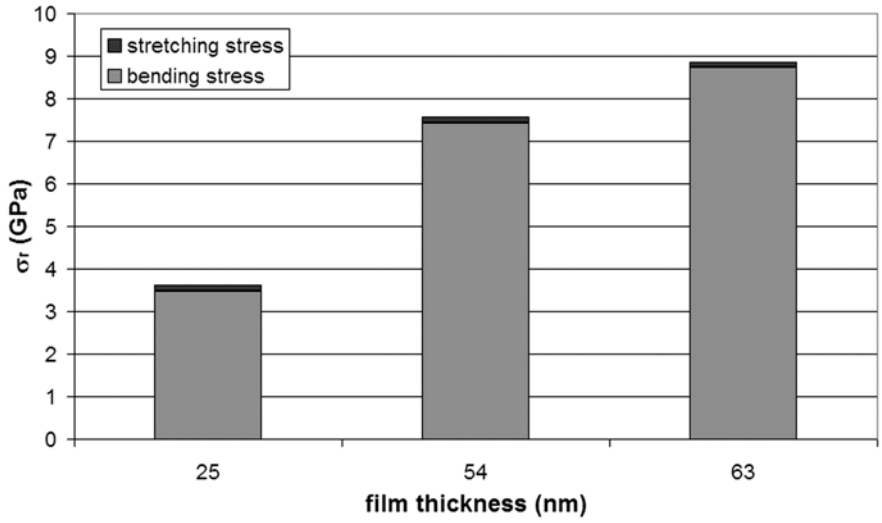

Figure 3-12 The total radial stress at fracture for the thermally grown oxide on the 1100Al mechanically polished substrate. The radial stress at fracture increased with film thickness and is dominated by the bending stress.

The oxide film on the mechanically polished 1100 substrate had a critical radial stress of 3.61 to 8.87 GPa for the 25 nm and 63 nm thick films. The membrane stress was found to stay constant for the different substrate materials and corresponding preparation technique. The membrane stress at failure depends on the critical depth, the plastic zone size, and the modulus of the film. The bending stress has a linear relationship with film thickness. Increasing the film thickness was the main contributor to the increase in radial stress at failure.

Discussion

The spherical cavity model under nanocontacts is an estimation into plastic zone size in the underlying substrate. The assumption made throughout the current study is that the through thickness cracking of the oxide films occurs at the plastic zone boundary. Physical observations for the location of the through thickness cracking were made with

the use of a scanning electron microscope. Micrographs were taken of two indentations made into the anodized aluminum oxide (Figure 3-13). A circumferential crack occurred during loading for both indents outside the contact area of the tip. The spherical cavity model estimated the circumferential crack radius to be a) 2.77 and b) 2.82μm. The calculation for the radius is dependent on the load carried by the substrate even though both indents in figure 3-13 had same maximum applied load by the indenter. The load carried by the substrate at fracture for two indents is a) 1.94 and b) 2.00mN. The radius for the circumferential crack in micrograph 3-13a was 2.3 and 2.5μm and in figure 3-13b was 2.9 and 3.7μm, depending on where the measurement was made. The measurement for circumferential radius is reasonably similar to the estimation made by the spherical cavity model under nanocontacts.

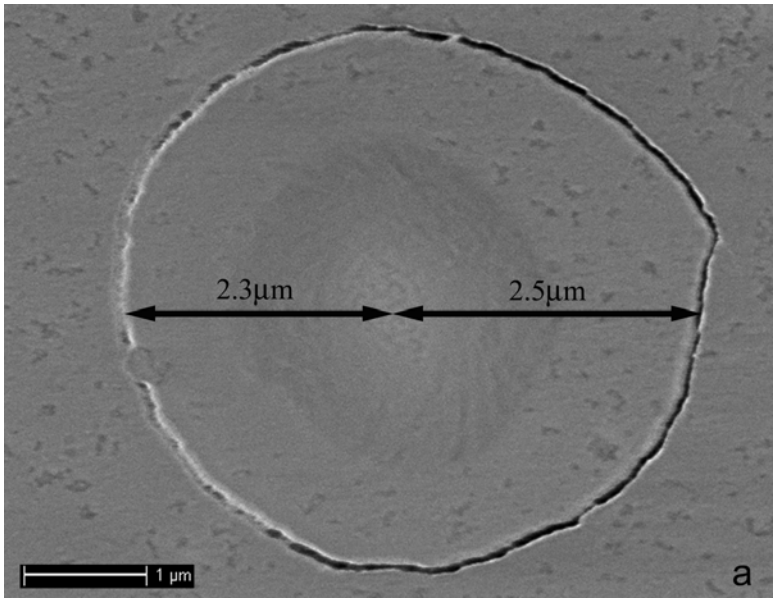

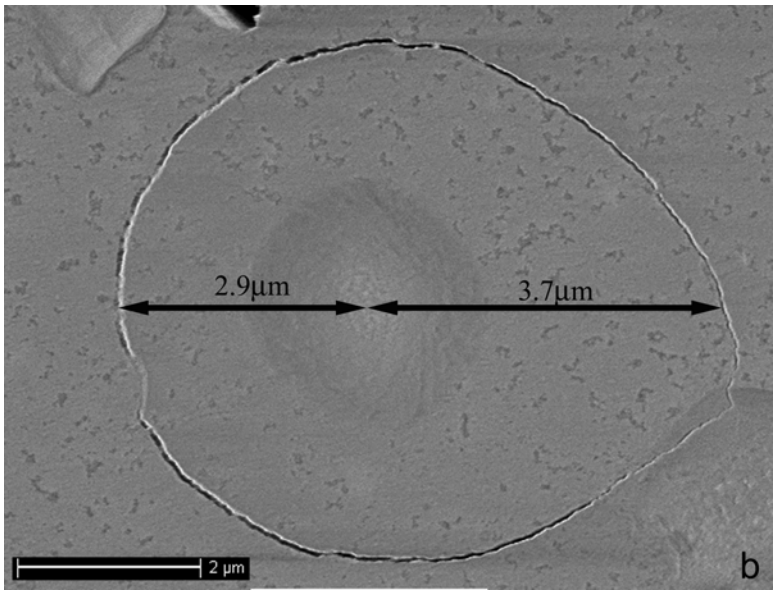

Figure 3-13 Physical observations of circumferential cracking measured a radius of a) 2.3 to 2.5µm and b) 2.9 to 3.7. The fracture radius was estimated to be a) 2.77 and b) 2.82µm using the spherical cavity model.

Surface flaws can greatly reduce the ultimate strength for thin films. These detrimental flaws are not necessarily well developed cracks. [60] However, a surface crack would be a worst case scenario. Propagation of the cracks could lead to a complete failure leaving the underlying metal exposed to the environment and loss of wear protection. A stress intensity factor can be calculated for a given material and crack dimension. Once the critical stress intensity factor has been reached the crack would propagate. Estimating the stress intensity at fracture for thin film applications would tell how much external load and what crack size would cause fracture.

The critical radial stresses showed that fracture of the thin film in this system was primarily caused from bending. The plate bending created a bending moment at the clamped edge of the flat circular plate (this model was previously used for estimating the radial stress). A schematic of the resulting bending moment can be seen in figure 3-14.

The overall applied load from the indenter tip is partially supported by the film and partially by the substrate. The load carried by the film does not influence the bending moment at the point of fracture. The only repulsive force, to the overall applied load by the indenter, that contributes to the bending moment is load supported by the underlying substrate.

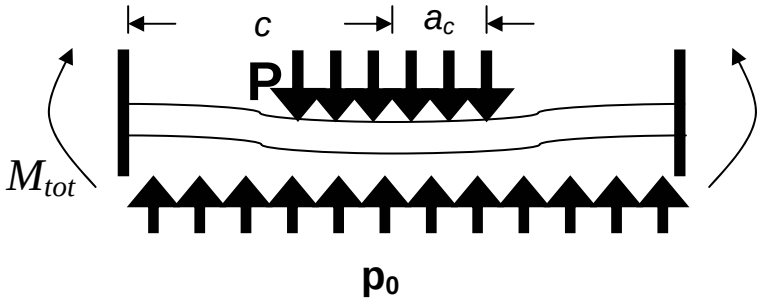

Figure 3-14 Schematic of the applied bending moment for a circular flat plate with clamped edges on a compliant foundation.

However, instead of using a point load (as was examined for the stress in the film) a more appropriate method is to assume that the contact load forms a circular projection on the film where the radius is less then the radius of the circular plate. For a first order approximation a uniformly loaded region corresponding to the contact area can be used (as shown in figure 3-14). While the actual loading profile follows elastic-plastic contact theories, the added complications of having an elastic film on a plastically deforming substrate make the imposition of a Hertzian pressure distribution challenging and as a starting approximation the uniformly loaded indentation radius will be used in this study. The bending moment M_θ can be estimated from [61]

$$M_\theta = \frac{P}{4\pi}(1+\nu)\left(\frac{a_c^2}{4c^2} - \ln\frac{a_c}{c}\right) \tag{18}$$

where P is the external applied load from the indenter, ν is poisson's ratio, a_c is the contact radius, and c is the radius of the circular plate (in this case it is the plastic zone radius).

There is also a second moment produced from the substrate applying a repulsive force that was opposite in direction of the indenter load. The moment created by the substrate M_{sub} can be modeled as a uniformly loaded circular plate [61]

$$M_{sub} = \frac{p_0 c^2}{8} \tag{19}$$

where p_0 is the uniform pressure carried by the substrate. The total moment acting at the clamped edge of the plate is a superposition of the two moments acting on the film.

$$M_{Tot} = M_{\theta} - M_{sub} \tag{20}$$

A first order approximation of the stress intensity factor can be calculated from the total bending moment produced at the clamped edge. Neglecting the radial force, because there is minimal stretching of the film from the contact load and assuming the residual stress is negligible, the stress intensity factor is [62]

$$K = \sigma\sqrt{\pi a}F\left(a/h_f\right) \tag{21}$$

where a is length of the surface crack, σ is the stress in the film at the clamped edge and $F(a/h_f)$ is a correction function taking the film thickness and the crack size into account. [62] Since the hardness of the substrate is about 200 MPa (corresponding to a tensile strength of about 75 MPa), the total residual stress which could develop in the system would be mitigated by plastic deformation in the underlying aluminum during cooling. As these stresses are much lower than those imposed by the indentation, to first order they will be ignored. The stress at the plate edge can be calculated by [62]

$$\sigma = \frac{6M_{tot}}{h_f^2} \tag{22}$$

Physical measurements of the initial crack size could not be measured due the surface topography of the oxide, only an estimate of this size can be made by examining the roughness of the samples. Pre-existing surface flaws would have a distribution of sizes and orientations. The critical surface flaw would be oriented perpendicular to the radial stresses. Therefore, to a first order, the applied stress intensity at fracture will be calculated using a constant a/h_f and then by varying a/h_f.

The applied stress intensity factor for a constant normalized critical crack size of 0.3 can be seen in figure 3-15. The stress intensity factor was highest for thinner films and decreased asymptotically towards a critical value for thicker films for all three substrates. The applied stress intensity factor for the thermally grown oxide on the 1100 mechanically polished, 1100 electropolished, and the 99.99% pure Al substrate were 0.17, 0.32, and 0.57 $MPam^{1/2}$, respectively, for the thicker films.

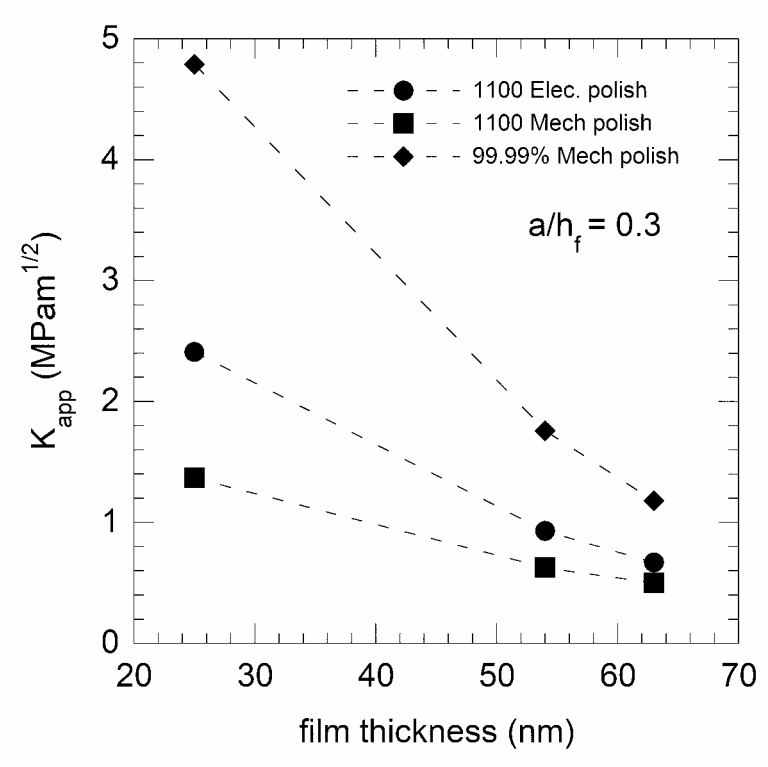

Figure 3-15 Applied stress intensity factor at fracture in the aluminum oxide – aluminum system assuming a constant normalized crack size of 0.3.

The surface crack size and orientation to the indent has a large affect on the applied stress intensity factor. The influence of the crack size was approximated by normalizing it to the film thickness. Figure 3-16 shows the relationship between the stress intensity factor for various substrates and crack sizes. For a given crack size to film thickness ratio the 99.99% mechanically polished aluminum substrate had the largest applied stress intensity factor and the 1100 mechanically polished substrate was found to have the smallest. The applied stress intensity at fracture for a crack length to film thickness ratio of 0.04 for the 54 nm thick film was 0.62, 0.32, and 0.22 $MPam^{1/2}$ for the oxide film on the 99.99% pure, 1100 electropolished, and 1100 mechanically polished, respectively. As the ratio of crack size to film thickness increased to 0.30 the stress

intensity increased to 1.76, 0.93, and 0.63 $MPam^{1/2}$ for the oxide film on the 99.99% pure, 1100 electropolished, and the 1100 mechanically polished substrates, respectively. These values for the stress intensity factor are reasonable for brittle ceramics.

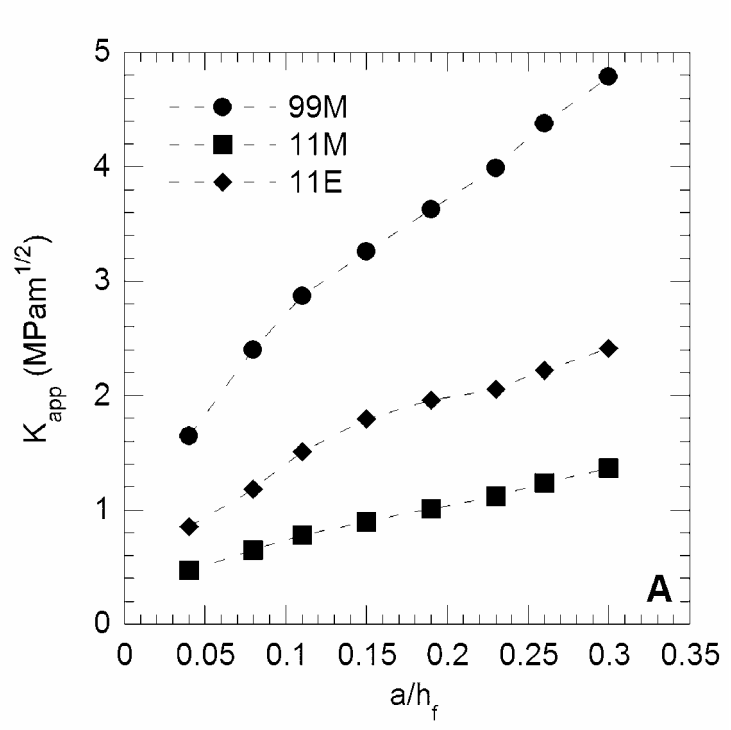

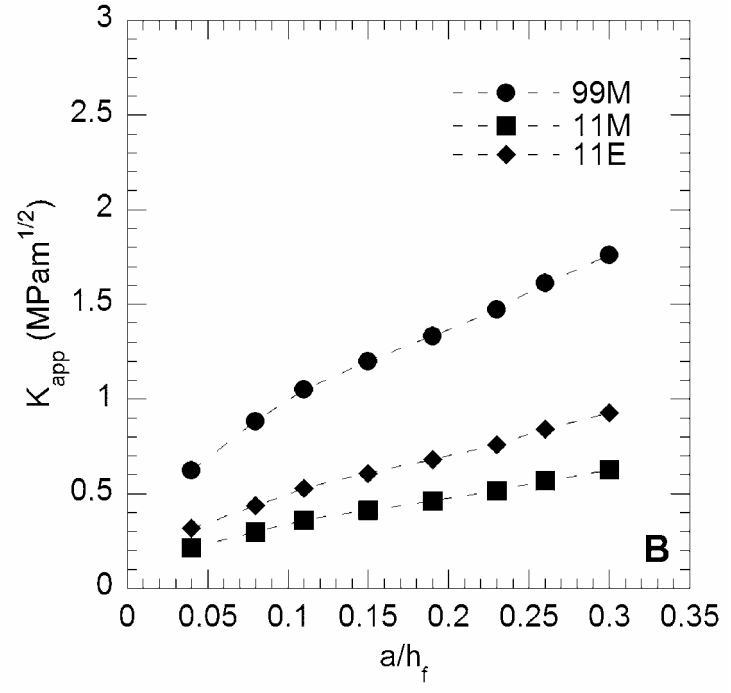

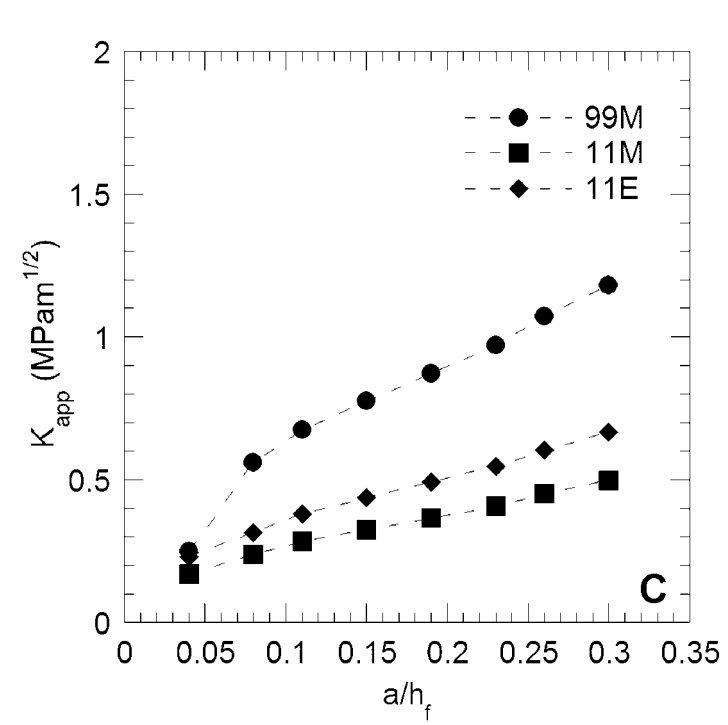

Figure 3-16 Applied stress intensity factor at fracture for various a/hf values for the a) 25 nm b) 54 nm and c) 63 nm thick films

In determining the critical parameters for film fracture, Chechenin *et al* considered the film as an elastic film on a yielding substrate and used the bending of circular clamped-edge plate with constant pressure acting from the substrate and a contact force from the indenter that increases towards the center. [35] This model is the same as the current study. However, Chechenin *et al* found that the film deflection was comparable to the film thickness. The bending moments were neglected and only considered the membrane force for failure. The current study showed that for this current system the film deflection was less than the film thickness and that the bending moments dominate the failure.

Weppelmann and Swain conducted a similar experiment using micro-indentation to determine a fracture criterion for hard films deposited on compliant substrates by

physical vapor deposition. It was shown that film failure was caused by large tensile stresses in the surface region outside the contact radius. [46] The large tensile stress at the surface for thin films was proven by Chai and Lawn using finite element analysis. [47] The representative curves for mode I stress intensity factor against a/h_f showed the same trends as the current study. Mode II fracture was neglected due to the small shear stresses created during indentation.

Reference:

[35] N.G. Chechenin, J. Bottiger, and J.P. Krog: Nanoindentation of amorphous aluminum oxide films II. Critical parameters for the breakthrough and a membrane effect in thin hard films on soft substrates, *Thin Solid Films* **261**, 228-235 (1995)

[36] M. Pang and D.F. Bahr: Thin-film fracture during nanoindentation of a titanium oxide film-titanium system, *J. Mater. Res.* **16**, 2634-2641 (2001)

[37] T.F. Page, W.C. Oliver, and C.J. McHargue: The deformation behavior of ceramic crystals subjected to very low load (nano) indentations, *J. Mater. Res.* **7**, 450-473 (1992)

[38] S.K. Venkataraman, D.L. Kohlstedt and W.W. Gerberich: Continuous microindentation of passivating surfaces, *J. Mater. Res.* **8**, 685-688 (1993)

[39] D.E. Kramer, K.B. Yoder, and W.W. Gerberich: Surface constrained plasticity: oxide rupture and the yield point process, *Phil. Mag. A* **81**, 2033-2058 (2001)

[40] D.F. Bahr, C.L. Woodcock, M. Pang, K.D. Weaver, and N.R. Moody: Indentation induced film fracture in hard film – soft substrate systems, *Inter. J. Frac.* **119/120**, 339-349 (2003)

[41] D. Rodriquez – Marek, M. Pang and D.F., Bahr: Mechanical Measurements of passive film fracture on an austenitic stainless steel, *Metal. Mater. Trans. A* **34A**, 1291-1295 (2003)

[42] S.V. Hainsworth , M.R. McGurk, and T.F. Page: The effect of coating cracking on the indentation response of thin hard coated systems, *Surf. Coat. Tech.* **102**, 97-107 (1998)

[43] R. Andersson, G. Toth, L. Gan, and M.V. Swain, Indentation response and cracking of sub-micron silica films on a polymeric substrate, *Eng. Fract. Mech.* **61**, 93-105 (1998)

[44] M.R. McGurk, H.W. Chandler, P.C. Twigg and T.F Page: Modelling the hardness response of coated systems: the plate bending approach, *Surf. Coat. Tech.* **68/69**, 576-581 (1994)

[45] W.W. Gerberich, A. Strojny, K. Yoder and L-S. Cheng: Hard protective overlayers on viscoelastic-plastic substrates, *J. Mater. Res.* **14**, 2210-2218 (1999)

[46] E. Wepplemann and M.V. Swain: Investigation of the stresses and stress intensity factors responsible for fracture of thin protective films during ultra-micro indentation tests with spherical indenters, *Thin Solid Films* **286**, 111-121 (1996)

[47] H. Chai and B.R. Lawn: Fracture mode transitions in brittle coatings on compliant substrates as a function of thickness, *J. Mater. Res.* **19**, 1752-1761 (2004)

[48] D.W. Aylmore, S.J. Gregg, W.B. Jepson: The oxidation of aluminum in dry oxygen in the temperature range 400-650 °C, *J. Inst. Metals* **88**, 205-208 (1959)

[49] E.A. Gulbransen and W.S. Wysong: Thin oxide films on aluminum, *J. Phys. Colloid Chem*., **51**, 1087-1103 (1947)

[50] L.P.H Jeurgens, W.G. Sloof, F.D. Tichelaar, and E.J. Mittemeijer: Structure and morphology of aluminum-oxide films formed by thermal oxidation of aluminum, *Thin Solid Films* **418**, 89-101 (2002)

[51] K.L. Johnson: *Contact Mechanics*, (Cambridge University Press, Cambridge, U.K., (1985)

[52] N.Q. Chinh, Gy. Horvath, Zs. Kovacs, and J. Lendvai: Characterization of plastic instability steps occurring in depth-sensing indentation tests, *Mater. Sci. Eng. A* **324**, 219-224 (2002)

[53] M.Y. He, A.G. Evans, and J.W. Hutchinson: The Ratcheting of compressed thermally grown thin films on ductile substrates, *Acta Mater***. 48**, 2593-2601 (2000)

[54] V.K. Tolpygo and D.R. Clarke: Wrinkling of α-alumina films grown by thermal oxidation I. Quantitative studies on single crystals of Fe-Cr-Al alloy**,** *Acta Mater***. 46** 5153-5166 (1998)

[55] D. Kramer, H. Huang, M. Kriese, J. Robach, J. Nelson, A. Wright, D. Bahr, and W.W. Gerberich: Yield strength predictions from the plastic zone around nanocontacts, *Acta Mater.* **47**, 333-343 (1998)

[56] S.V. Hainsworth, H.W. Chandler, and T.F. Page: Analysis of nanoindentation load-displacement loading curves, *J. Maters. Res.* **11**, 1987-1995 (1996)

[57] S. Timoshenko and S. Woinowshy-krieger: *Theory of plates and shells*, Mcgraw-Hill, New York (1959)

[58] W.D. Kingery, H.K. Bowen, and D.R. Uhlman, *Introduction to Ceramics 2nd Ed.*, Wiley, New York, 777 (1976)

[59] G.W.C. Kaye and T.H. Laby, *Tables of Physical and Chemical Constants*, 14th ed., Longman, London, 31 (1973)

[60] B.R. Lawn: Fracture and deformation in brittle solids: A perspective on the issue of scale, *J. Mater. Res.* **19**, 22-29 (2004)

[61] J.P. Den Hartog: *Advanced strength of Materials*, Dover Publications Inc., New York (1952)

[62] G.C. Sih: *Handbook of Stress Intensity Factors*, Lehigh University, Bethlehem, PA (1973)

Chapter 4

Energy method to analyze through thickness thin film fracture

Hard thin films on soft substrates, such as Al_2O_3 on Al and TiO_2 on Ti, readily form on the surface under ambient conditions. In addition these films can be grown by anodic methods to produce desirable properties for wear or corrosion resistance. Mechanical breakdown of these films can cause premature failure of the substrate. The most common types of mechanical testing of these films are scratch or peel testing.

Recently, nanoindentation has been used to test the mechanical properties of hard thin films such as the elastic modulus and hardness. Nanoindentation can also be used to test the film's toughness by inducing fracture in the film upon loading. The fracture of the film can result in a discontinuity in the load-depth curve. Thin films have been show to fracture at critical loads and depths. [63] Previous studies have analyzed these fracture events has been analyzed by calculating an applied radial stress [64-66], an applied stress intensity at fracture [66-69] and the amount of energy required to produce cracks in the film. [70-75]

A critical amount of energy is required to fracture a thin film. This energy can be determined by producing a load depth curve from nanoindentation until fracture occurs. The total energy applied during the indentation can calculated by simply integration to the fracture depth. The energy used to plastically deform the substrate must be subtracted from the total energy, leaving the amount of energy needed to fracture the thin film.

Malzbender and de With [70] demonstrated that the dissipated energy during indentation was related to the fracture toughness of the coating and interface by performing simple integrations of the loading and unloading portions from indentation to

determine the amount of energy needed to damage the film. The films that they produced were shown to delaminate and chip along with through thickness fracture in the film. The energy needed for delamination and chipping was then calculated. The crack extension force was then used to calculate the interfacial stress intensity and critical stress intensity for fracture. The plastic deformation in substrate was not taken into account, this will lead to an overestimation of the energy release rate.

Other studies have suggested that the fracture energy could be estimated as the energy consumed during the first circumferential crack during the load drop or plateau on the load-displacement curve. [69,71,73,76] Three different methods have discussed estimation methods for the fracture energy from the load-depth curves. Li *et al* [73] suggested an approach based on the idea that the total energy released during crack initiation is the fracture energy divided by the new surface area. The total energy measured from the load-depth curve was determined by extrapolating the loading curve from the beginning of the excursion to the end. The energy method from Li *et al* is represented by the area in quadrilateral ABCD in figure 4-1. Work performed by van der Varst and de With [71] used an internal variable theory to separate the different activities that produce total dissipated energy. The extent of damage at the interface, plastic deformation in the system, damage in the system, and the generation of heat were taken into account. They used such internal variables as crack length, plastic strain, and degree of micro damage to derive a work function that only depended on the initial and final states to determine the energy. The surface roughness was found to increase the scatter in the data. However, the data was seen to follow a master curve. The indentation in the sample produced circumferential cracking outside the contact area of the tip. The work

from the ring cracking was calculated by multiplying the load at the discontinuity by the discontinuity length and dividing by the surface area of the crack. This method can be represented on the load-depth schematic (figure 4-1) as the area in triangle OAC. This does not take into account the effects from the substrate and the energy calculated is an overall dissipated energy from the system, not just the film. The third energy method suggested by Abdul-Baqi and Van der Giessen [72] was to multiply one half of the cracking depth by the load jump. This method is represented by the area in triangle OAD in figure 4-1.

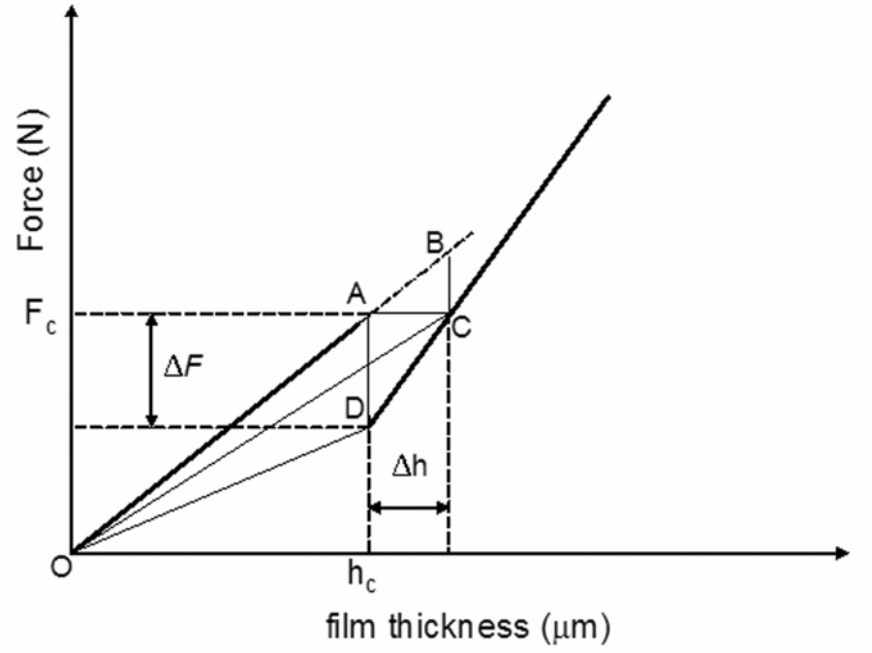

Figure 4-1 Schematic load depth curves used for fracture energy estimations. The energy estimations for Abdul-Baqi is outlined as OAD, Van der Varst and de With is OAC, and Li et al is ABCD.

Numerical simulations performed by Abdul-Baqi and van der Giessen demonstrated that the energy determination by Li *et al* was found to underestimate the overall energy for small and fracture energies and small film thicknesses, where the methods by Abdul-Baqi *et al* and van der Varst *et al* were reasonable estimations.

However, the second and third methods overestimate the overall energy for large fracture energies and large film thicknesses. The problem with these methods is that the loading is assumed to be linear with depth. However, the indentation follows elastic-plastic contact theories where the load and depth have a power law relationship. [77,78] Also, substrate effects were not taken into account for any of the above methods to determine the energy to initiate a crack.

The current study will outline a method to separate the energy dissipated from fracture of the film and the energy dissipated to plastically deform the substrate. Being able to separate these energies from the total energy applied by the nanoindenter allows a determination of the energy release rate for film fracture and calculating the critical stress intensity factor under plane stress.

Experimental Procedure

Grade II polycrystalline titanium with a primarily α HCP grain structure was ground to 600 grit and then mechanically polished using 0.05 μm colloidal silica. A thin oxide was then anodically grown using an EG&G 173 and 175 potentiostat and controller. The film was grown in a 0.1 M H_2SO_4 solution. The final potential was reached using step polarization. The potential was increased by 1V every few minutes (once the current density stabilized at each potential) until a maximum of 9.4V was reached. The potential was measured against an Ag/AgCl reference electrode and a graphite counter electrode. The sample was then held at the maximum potential for 5min. The titanium oxide thickness was determined using x-ray photoelectron spectroscopy (XPS) depth profiling. A sputtering rate of 35 angstroms per minute was used. The

thickness of each oxide was measured by determining the depth at which the oxygen is 50% of its maximum concentration. The film thickness was found to be 200nm.

Two different aluminum substrates were also tested in this study. The samples were made from a commercially available ingot of 1100 aluminum and a 99.99% pure Al ingot. The substrates were encapsulated in an evacuated quartz tube, back filled with argon gas and annealed at 500°C for 24 hrs.

After annealing, the aluminum samples were polished. The polishing techniques and film growth methods for the thermally grown aluminum oxide films are as described in the experimental techniques section in chapter 3. The oxide thickness was not influenced by the underlying substrate in these materials. Gulbransen and Wysong [79] studied the growth of aluminum oxide on aluminum and over a temperature range of 400 to 500°C. The oxide layer was found to be amorphous in structure but the heating time was only 30 min. [79,80]

Nanoindentation was carried out using a Hysitron Triboscope coupled with a Park Autoprobe scanning probe microscope. The indentations were made with a cube corner diamond indenter (90° included angle) with an effective tip radius of 570 nm. The tip radius was calculated by performing a series of elastic loading curves in tungsten. The tip radius was then calculated from the elastic curves using the Hertzian elastic loading profile. [77] The indentation curves were load controlled until a maximum load of 5000μN.

Results

The hardness of the aluminum substrate and the grade II polycrystalline titanium were determined through nanoindentation with a maximum load of 900 μN and 6000μN,

respectively. The average hardnesses for the aluminum and titanium substrates are 200 MPa and 2.41 GPa, respectively. The hardness values were calculated from 15 indents at various locations in the polycrystalline samples. No discontinuities were present on the load-depth curves for the both substrates. The yield stress can be estimated using Tabor's relationship between the hardness, H and yield stress, σ_y.

$$\sigma_y = \frac{H}{3} \tag{23}$$

The yield stress was determined to be 75 MPa and 800 MPa for the aluminum and titanium, respectively. A curve fit operation was then used to determine the loading profile of the titanium substrate. The loading curve follows a power law relationship and was curve fit using [78]

$$P_s = K\delta^n + C \tag{24}$$

where P_s is load applied to the substrate, K, n and C are empirical constants, and δ is the depth of penetration. The resulting load-depth curves from the indentations made into the anodized showed discontinuities. The load-depth curves from the substrates did not contain any discontinuities. Two typical load-depth curves, one from the anodized titanium and one from the titanium without a film, can be seen in figure 4-2. The titanium sample without the film was shown to reach higher penetration depths at low loads than the anodized sample. The load -depth curve for anodized titanium was clearly affected by the presence of titanium oxide on the surface.

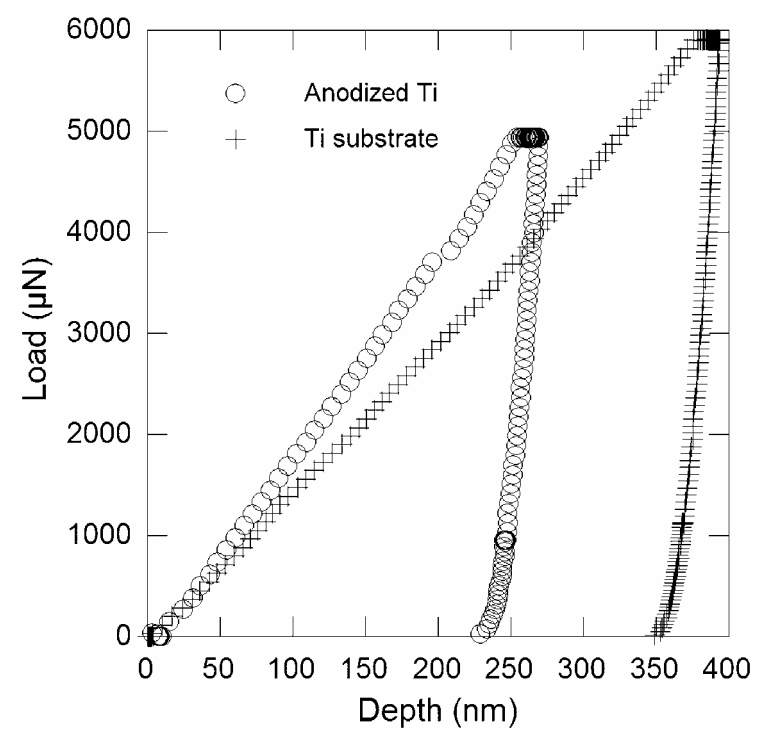

Figure 4-2 Load-depth results from indentations into grade II polycrystalline Ti with and without an anodized film

Nanoindentation was also performed on an anodized aluminum substrate, using a tip with a larger radius (approximately 1 μm) and a film that is thicker than the thermally grown oxides, approximately 150 – 250 nm thick. A discontinuity at 8mN was caused from a circumferential crack that occurred outside of the tip contact radius. The circumferential crack around the indentation can be seen in figure 4-2. The contact radius is labeled as a_c and the radius of the circumferential crack is labeled as c. Circumferential cracks were not present around indentations made with a maximum load of 7mN. The anodized film was utilized to demonstrate the circumferential cracking because the film's surface was smooth compared to the thermally grown oxides.

Discussion

The position of the through thickness cracks are located at the elastic-plastic boundary in the substrates. [65] The film covering the plastic region is allowed to deform. The film beyond the plastic zone is held in place during indentation. Estimation to the plastic zone radius under nanocontacts has been shown to be [81]

$$c = \sqrt{\frac{3P_s}{2\pi\sigma_y}} \tag{25}$$

where P_s is the load carried by the substrate at the time just prior to fracture and σ_y is the yield stress of the substrate. The radial plastic zone will result in circumferential cracking of the film outside the contact area of the tip. Scanning electron micrographs, which are shown in figure 3-13, show that the spherical model for the plastic zone radius is a good estimation to the location of the through thickness fracture of the oxide films. A schematic for the position of the through thickness crack can be seen in figure 4-3.

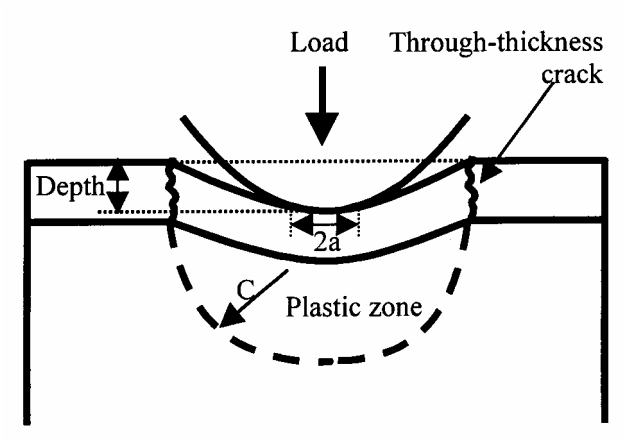

Figure 4-3 schematic of through thickness cracking of the thin film

Simple integration of the load-depth curves produced during indentation result in the energy that was put into the system. Integration of the load-depth curves, from the

anodized film, until the onset of fracture (beginning of the discontinuity) will give the total energy applied, *U*.

$$U = \int_0^{\delta_c} P(\delta) d\delta \tag{26}$$

This includes energy participating in deformation of the substrate and film. The energy does not decipher between elastic or plastic deformation. The area of integration for the anodized film and titanium substrate is shown in figure 4-4.

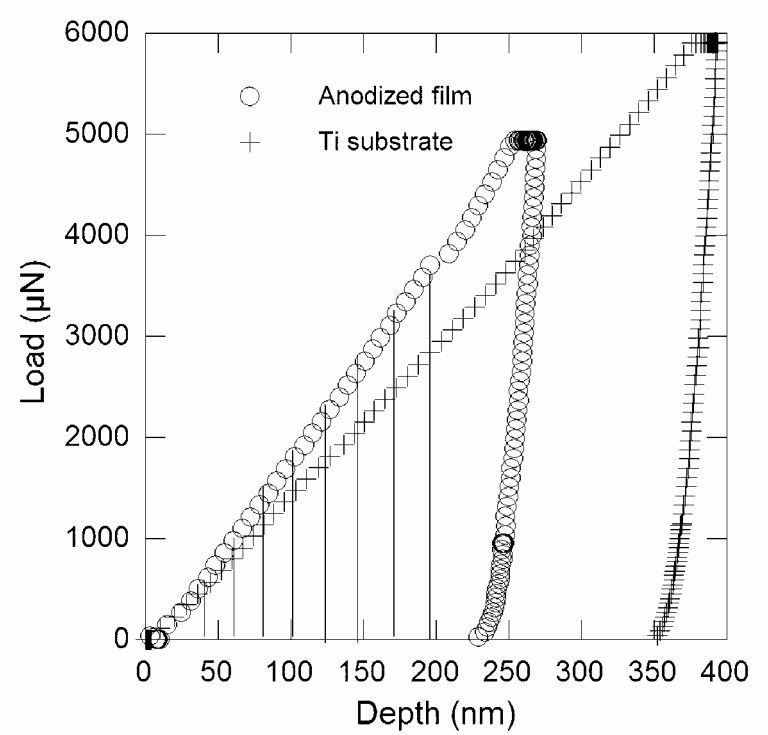

Figure 4-4 Energy applied to the system during indentation of the anodized titanium

The total energy put into the system is a superposition of the energy to fracture the film and the energy to plastically deform the substrate. An integration of the resulting load-depth curves from the titanium prior to anodizing gave estimation into the amount of energy needed to plastically deform the substrate. The integration was conducted until the

critical depth at fracture occurred for the anodized titanium. The amount of energy needed to fracture the film, U_{film} can then be determined by subtracting the energy for plastic deformation of the substrate, $U_{substrate}$ from the total energy applied to the system, U_{system}. The superposition of energies from the film and substrate can be seen in figure 4-5.

$$U_{film} = U_{system} - U_{substrate} \tag{27}$$

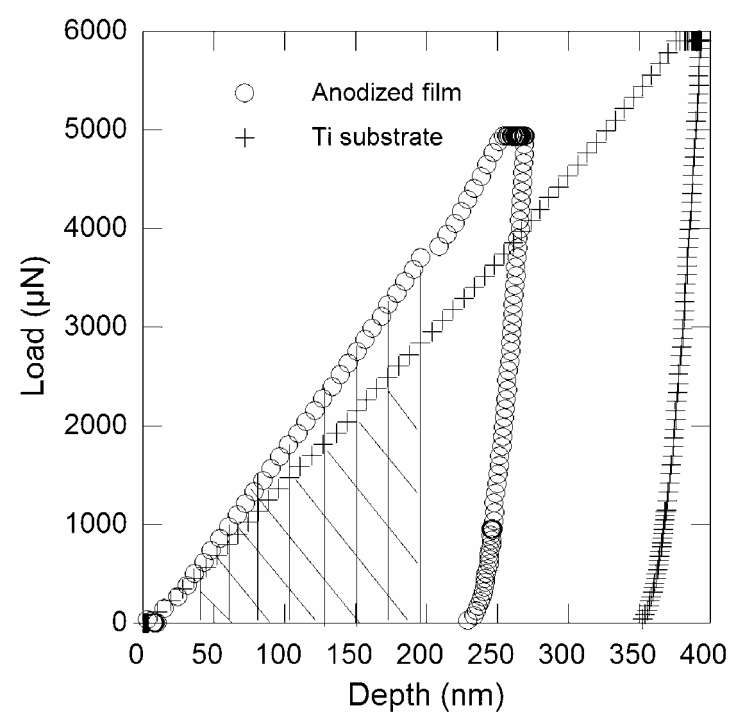

Figure 4-5 The energy to fracture the film determined by substracting the energy to deform the substrate from the entire system

The energy to fracture the titanium oxide films were shown to range by an order of magnitude. The energy for fracture is dependent on the thickness of the film and the location of where the crack initiates. The energy is dependent on the new area produced from the formation and propagation of the crack. Table 4-1 summarizes the average energy needed for fracture for each film thickness and substrates.

Table 4-I Energy results for thermally grown oxides (TGO) on various aluminum substrates and an anodized titanium

Sample	h_f (nm)	U_{system} (pJ)	U_{film} (pJ)
1100Al Mech polish (TGO)	25	0.093 +- 0.032	0.052 +- 0.031
	54	0.133 +- 0.048	0.072 +- 0.017
	63	0.121 +- 0.074	0.079 +- 0.052
1100Al Electropolish (TGO)	25	0.073 +- 0.034	0.052 +- 0.024
	54	0.098 +- 0.018	0.066 +- 0.035
	63	0.103 +- 0.059	0.071 +- 0.033
99.99%Al Mech polish (TGO)	25	0.179 +- 0.105	0.122 +- 0.078
	54	0.260 +- 0.138	0.136 +- 0.095
	63	0.274 +- 0.188	0.104 +- 0.56
Anodized Titanium	250	249.7 +- 130 .1	74.69 +- 37.89

The methods outlined by van der Varst *et al* [71] and Abdul-Baqi *et al* [72] to determine fracture energy was shown to be reasonable for thin films. The thermally grown oxide with a thickness of 63 nm on the electropolished aluminum substrate was found to have an average fracture energy of 0.070 pJ with a standard deviation of 0.061 pJ using the method outlined by van der Varst. The method outlined by Abdul-Baqi calculated an average fracture energy of 0.056 pJ with a standard deviation of 0.039 pJ. The method in the current work resulted in an average fracture energy of 0.071 pJ and a standard deviation of 0.033 for the same system. This similarity, which may at first be taken as encouraging, is likely more fortuitous than not, because the three methods (that described in Fig. 4-5, Abdul-Baqi, and that of van der Varst) are inherently different measurements of energy.

In thin film fracture, we will assume a crack is initiated and propagates completely through the thickness. It takes a certain amount of force to move the crack front. In thin film fracture a crack is initiated and propagates completely through the thickness. The surface area of the crack is the circumference of the crack multiplied by the thickness of the film. The energy can then normalized by the area of the crack. This

will result in the crack extension force for the film. The equation for the crack extension force is

$$G = \frac{U_{film}}{4\pi c h_f} \tag{28}$$

where c is radius of plastic zone and h_f is the film thickness. The plastic zone radius was determined from the load applied to the substrate. The denominator is multiplied by 2 because there are two new surfaces being created during the crack extension. The equation for the crack extension force was modeled for a constant load condition for fracture. The crack extension force for the titanium oxide film is 19.75 J/m^2. The crack extension force for the different aluminum oxide thicknesses on various aluminum substrates and the anodized titanium is summarized in table 4-II. The elastic modulus used to calculate the stress intensity at fracture for the thermally grown aluminum oxide and anodized titanium oxide was 411 GPa and 180 GPa, respectively. This elastic modulus for the thermally grown aluminum oxide and titanium oxide is considered to be an upper bound because they were taken from their crystalline structures. The thermally grown oxide films may have an amorphous structure. Amorphous materials typically have lower elastic modulus than its crystalline form. The elastic modulus for the anodized aluminum was 140 GPa. [82]

Table 4-II Calculated results for crack extension force (G) and stress intensity at frature (K_{app}) for the oxide films grown on various aluminum substrates and an anodized titanium

Sample	h_f (nm)	G (J/m^2)	K_{app} (MPam$^{1/2}$)
1100Al Mech polish (TGO)	25	0.96 +- 0.53	0.64 +- 0.16
	54	0.59 +- 0.14	0.51 +- 0.06
	63	0.56 +- 0.34	0.48 +- 0.15
1100Al Electropolish (TGO)	25	0.63 +- 0.30	0.52 +- 0.13
	54	0.34 +- 0.18	0.37 +- 0.12
	63	0.32 +- 0.09	0.38 +- 0.05
99.99%Al Mech polish (TGO)	25	1.67 +- 0.95	0.83 +- 0.25
	54	0.74 +- 0.49	0.55 +- 0.20
	63	0.49 +- 0.40	0.45 +- 0.14
Anodized Titanium oxide	200	19.8 +- 7.74	2.51 +- 0.51
Anodized Aluminum oxide	200	0.31 +- 0.03	0.22 +- 0.01

Figure 4-6 shows the resulting crack extension force for the 25, 54, and 63 nm thick oxide films on the various aluminum substrates. Each point on the graph is an average of 10 indents randomly positioned on the sample. The standard deviation shows that there is some overlap in data from the 25 nm thick film to the 64 nm thick film. The standard deviation for the crack extension force, for a given film thickness, overlapped. This shows that no matter what substrate was used for the thermally grown aluminum the crack extension force was equivalent. Since it takes a critical amount of energy for a crack to propagate the crack extension force has to approach a critical value. From the data given a critical value for the crack extension force could not be deduced. The average crack extension force for the aluminum oxide ranged from 0.32 to 1.67 J/m^2 for the various thicknesses and substrates. The anodically grown aluminum oxide film was found to have a fracture energy of 0.31 J/m^2. Polycrystalline sapphire was shown to have fracture energies between 6 and 7.3 J/m^2. [83] The crack extension force for the 250 nm thick titanium oxide film was 19.8 J/m^2 with a standard deviation of 7.74 J/m^2. A general

study of bulk titanium oxide fracture toughness measured a fracture energy of 68 J/m^2. [84]

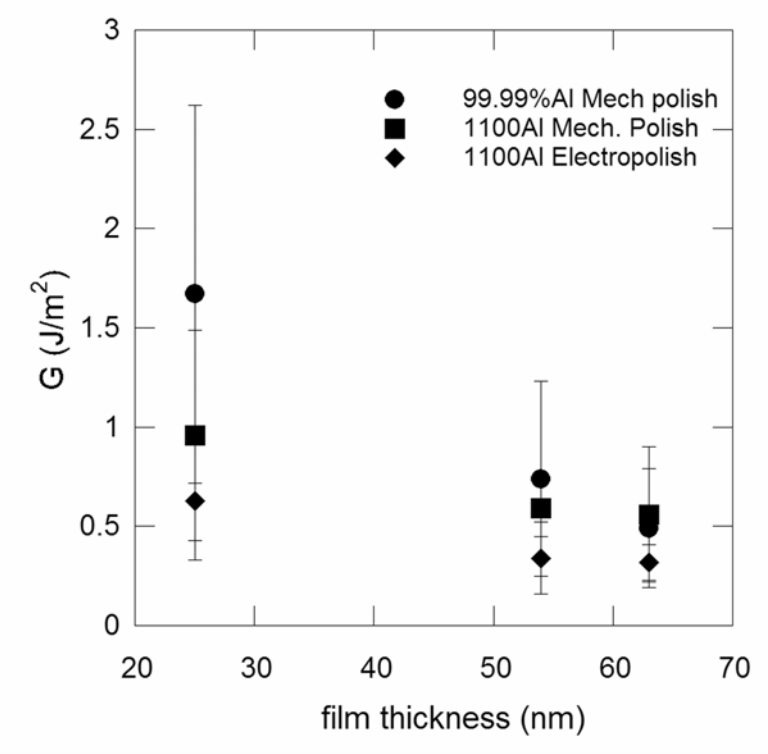

Figure 4-6 Resulting crack extension forces from 25, 54, and 63 nm thick oxide films on various aluminum substrates

The crack extension force is fracture criterion from an energy basis. There is a correlation between the energy method and the stress intensity method. It is reasonable to assume the thin films are in a state of plane stress. The correlation between the crack extension force and stress intensity, for plane stress, is

$$K = \sqrt{GE} \tag{29}$$

where E is the plane strain elastic modulus of the film. The elastic modulus of titanium oxide thin films was shown to vary between 65 GPa and 147 GPa for films produced by reactive evaporation and ion plating, respectively. [85] The elastic modulus for sintered

polycrystalline plates of titanium dioxide is on the order of 185 GPa and rutile varied between 120 GPa and 480 GPa, depending on crystal orientation. [86,87] An elastic modulus of 180 GPa was chosen for the anodically grown titanium oxide thin film. This gives two different methods for determining fracture. The stress intensity at fracture could be related back to the stress applied to the film and the size of a critical flaw. [65] Table 4-2 summarizes the applied stress intensity at fracture calculated from the crack extension force. Figure 4-7 illustrates the applied stress intensity at fracture for the varying aluminum oxide thicknesses and aluminum substrates.

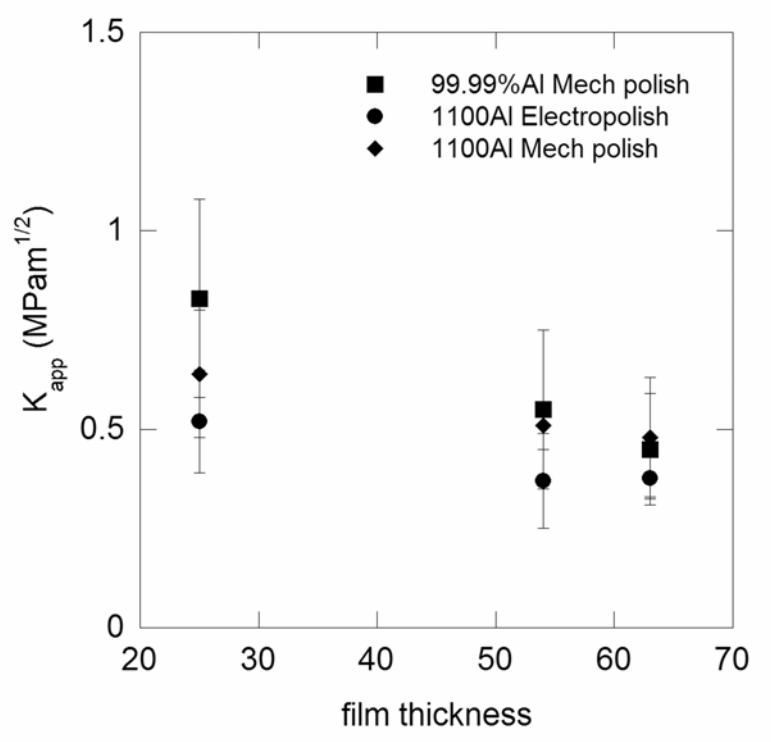

Figure 4-7 Resulting stress intensity values at fracture for 25, 54, and 63 nm thick oxide films on various aluminum substrates

Similar to the crack extension force the results for the applied stress intensity show that standard deviation from the average overlap no matter what the thickness of the oxide or substrate that the film was grown on. The asymptotic behavior for the stress

intensity at fracture as the film increases from the energy approach (figure 4-7) is similar to the graph of the stress intensity at fracture from the plate bending approach where the ratio of defect size to film thickness was held constant (Figure 3-14). This shows that the critical defect size in the thermally grown oxides increased with increasing film thickness. As the crack extension force has a critical value there is a critical value for the applied stress intensity for a crack to propagate. The stress intensity from the crack extension force calculations for the aluminum oxide thin film was between of 0.37 and 0.83 $MPam^{1/2}$. The anodically grown aluminum oxide was 0.22 $MPam^{1/2}$ with a standard deviation of 0.01. Single crystal sapphire has been shown using a controlled flaw fracture test to have fracture toughness values from 2.43 to 4.54 $MPam^{1/2}$ depending on the plane and crystallographic direction the test was administered. [88] These values were obtained using a double cantilever beam fracture test in a nitrogen atmosphere. Fracture testing of single crystal sapphire using indentation has shown that it has fracture toughness between 1.89 and 2.55 $MPam^{1/2}$. [89] The titanium oxide film was shown to have a stress intensity of 2.51 $MPam^{1/2}$ with a standard deviation of 0.51 $MPam^{1/2}$. A general study of bulk titanium oxide fracture determined the fracture toughness to be 6.1 $MPam^{1/2}$. [84] The fracture energies and applied stress intensity at fracture for the aluminum oxide and titanium oxide thin films were comparable to the bulk properties. The properties for the thin films were slightly lower than the bulk properties.

Reference:

[63] N.G. Chechenin, J. Bottiger and J.P. Krog: Nanoindentation of amorphous aluminum oxide films II. Critical parameters for the breakthrough and a membrane effect in thin hard films on soft substrates, *Thin Solid Films* **261**, 228-235 (1995)

[64] M. Pang and D.F. Bahr: Thin-film fracture during nanoindentation of a titanium oxide film-titanium system, *J. Mater. Res.* **16**, 2634-2641 (2001)

[65] D.F. Bahr, C.L. Woodcock, M. Pang, K.D. Weaver, and N.R. Moody: Indentation induced film fracture in hard film – soft substrate systems, *Inter. J. Frac.* **119/120**, 339-349 (2003)

[66] E. Wepplemann, and M.V. Swain: Investigation of the stresses and stress intensity factors responsible for fracture of thin protective films during ultra-micro indentation tests with spherical indenters, *Thin Solid Films* **286**, 111-121 (1996)

[67] J. Thurn and R.F. Cook: Mechanical and thermal properties of physical vapour deposited alumina films: Part II Elastic, plastic, fracture, and adhesive behaviour, *J. Mater. Sci.* **39**, 4809-4819 (2004)

[68] C. Herzl: Fracture mechanics analysis of thin coatings under plane-strain indentation, *Int. J. Sol. Struct.* **40**, 591-610 (2003)

[69] J. Malzbender, G. de With, and J.M.J. den Tooner: Elastic modulus, indentation pressure and fracture toughness of hybrid coatings on glass, *Thin Solid Films,* **366,** 139-149 (2000)

[70] J. Malzbender and G. de With: Energy dissipation, fracture toughness and the indentation load-displacement curve of coated materials, *Surf. Coat. Tech.* **135**, 60-68 (2000)

[71] P.G. Th. van der Varst and G. de With: Energy based approach to the failure of brittle coatings on metallic substrates, *Thin Solid Films* **384,** 85-89 (2001)

[72] A. Abdul-Baqi and E. Van der Griessen: Numerical Analysis of indentation-induced cracking of brittle coatings on ductile substrates, *Int. J. of Sol. Struct.* **39,** 1427-1442 (2002)

[73] X. Li, D. Diao, and B. Bhushan: Fracture mechanisms of thin amorphous carbon films in nanoindentation, *Acta Mater.* **45,** 4453-4461 (1997)

[74] K. Sriram, R. Narasimham, and S. Biswas: A numerical fracture analysis of indentation into thin hard films on soft substrates, *Eng. Fract. Mech*. **70** 1323-1338 (2003)

[75] Z. Xia, W. Curtin, B. Sheldon: A new method to evaluate the fracture toughness of thin films, *Acta. Mater*. **52,** 3507-3517 (2004)

[76] X. Li and B. Bhushan: Measurement of fracture toughness of ultra thin amorphous carbon films, *Thin Solid Films*, **315,** 214-221 (1998)

[77] K.L. Johnson: *Contact Mechanics*, (Cambridge University Press, Cambridge, U.K., (1985)

[78] S.V. Hainsworth, H.W. Chandler, and T.F. Page: Analysis of nanoindentation load-displacement loading curves, *J. Mater. Res*., **11** 1987-1995 (1996)

[79] E.A. Gulbransen and W.S. Wysong: Thin oxide films on aluminum*, J. Phys. Colloid Chem*., **51**, 1087-1103 (1947)

[80] L.P.H. Jeurgens, W.G. Sloof, F.D. Tichelaar, and E.J. Mittemeijer: Structure and morphology of aluminum-oxide films formed by thermal oxidation of aluminum, *Thin Solid Films* **418**, 89-101 (2002)

[81] D. Kramer, H. Huang, M. Kriese, J. Robach, J. Nelson, A. Wright, D. Bahr, and W.W. Gerberich: Yield strength predictions from the plastic zone around nanocontacts, *Acta Mater*. **47**, 333-343 (1998)

[82] G. Alcala, S. Mato, P. Skeldon, G.E. Thompson, A.B. Mann, H. Habazaki, K. Shimizu: Mechanical properties of barrier-type anodic alumina films using nanoindentation, *Surf. Coat. Tech*. **173**, 293-298 (2003)

[83] S.W. Wiederhorn: Fracture of sapphire, *J. Amer. Ceram. Soc*. **52**, 9, 485-491 (1969)

[84] W.P. Minnear and R.C. Bradt: Stoichiometry Effects on the fracture of TiO_{2-x}, *J. Amer. Ceram. Soc*. **63**, 485-489 (1980)

[85] O. Anderson, C. R. Ottermann, R. Kuschnereit, P. Hess, and K. Bange: Density and young's modulus of thin TiO2 films, Fresenius Journal of Analytical Chemistry **358**, 315-318 (1997)

[86] W.P Minnear and R.C. Bradt: Elastic properties of polycrystalline titanium oxide (TiO_{2-x}), *J. Amer. Ceram. Soc*. **60**, 458-459 (1977)

[87] M.H. Grimsditch and A.K. Ramdas: Elastic and elasto-optic constants of rutile from a Brillouin scattering study, *Phys. Rev*. **B14**, 1670-1682 (1976)

[88] M. Iwasa and T. Ueno: Fracture toughness of quartz and sapphire single crystals at room temperature, *Zairyo* **30**, 337, 1001-1004 (1981)

[89] G.R. Anstis, P. Chantikul, B.R. Lawn, and D.B. Marshall: A critical evaluation of indentation techniques for measuring fracture toughness: I direct crack measurements, *J. Amer. Ceram. Soc.* **64**, 9, 533-538 (1981)

Chapter 5

Conclusion and Recommendations

Two different methods for determining the stress intensity at fracture of the thin films using nanoindentation were outlined and tested. The method outlined in chapter 3 utilized a plate bending approach to determine the stress intensity at fracture. Chapter 4 discussed a method by measuring the energy at film fracture from the load-depth curves. The ability to incorporate two different metal oxide systems to the energy method implies that it could be universal for hard film soft substrate systems. The plate bending approach was only tested using the aluminum oxide/aluminum system. The results from the plate bending method were in good comparison to the stress intensity calculations from the energy method. The final results for both methods were reasonable values for the stress intensities and crack extension forces.

This plate bending method developed a first order analytical model for characterizing the stress intensity leading to thin film failure during nanoindentation, and applied this model to thermally grown oxide films on aluminum. The films were modeled as a thin elastic circular plate with clamped edges supported by a compliant substrate. In the aluminum oxide/aluminum system, the radial stress at fracture was calculated using a superposition of the bending and membrane stress. The bending stress was found to dominate the overall stress at fracture. The 63 nm films were determined to have ultimate strengths of 8.87, 4.77, and 6.21 GPa for the 1100 Al mechanically polished, 1100 Al electropolished, and 99.99% Al mechanically polished substrates, respectively.

The applied stress intensity factor was calculated from the bending moment produced during indentation. The radial force was neglected in the stress intensity factor

calculation due minimal deflection of the oxide at failure. As the ratio of crack size to film thickness increased to 0.30 (which is approximately the ratio of the roughness of the films to the total film thickness) the stress intensity at fracture increased to 1.76, 0.93, and 0.63 $MPam^{1/2}$ for the 99.99% pure mechanically polished, 1100 electropolished, and the 1100 Al mechanically polished substrates, respectively. It is interesting to note that the oxide the grown on the 99.99% pure aluminum substrate had the highest load at fracture and was shown to have the highest stress intensity at fracture. The reason for this is that the oxide film grown on the 99.99% pure aluminum substrate would have fewer trace elements producing a higher quality film. The 1100 aluminum substrate contains trace amounts of foreign elements that could be incorporated into the oxide during growth.

An energy based method was used to determine the toughness of brittle oxide films on metal substrates. The total energy being applied to the system is a superposition of the energy needed to deform the film and the substrate. The initial loading for the film/substrate system was steeper than the response from the substrate. The applied energy difference between the film/substrate system and the substrate alone was the energy applied to the film. The loading profile of both the film/substrates system and the substrate was then integrated up to the same critical depth as the system. Subtraction of the energy applied to the substrate from the system gives the fracture energy of the film. The crack extension force, or energy per unit area of crack surface, was determined by dividing the energy by newly acquired surface produced from crack initiation and propagation by using the relationship that the film is a high strength ceramic and it undergoes elastic deformation until fracture. The average crack extension force for the

various thicknesses and substrates ranged from 0.32 to 1.67 J/m^2. The stress intensity at fracture for the various aluminum substrates and oxide thicknesses ranged from 0.37 and 0.83 $MPam^{1/2}$. The average crack extension force and stress intensity at fracture for the 200 nm thick titanium oxide film was 19.8 J/m^2 and 2.51 $MPam^{1/2}$, repectively.

Defects in the films were the main contributor to fracture. The 25nm thick films were shown to fracture at the highest stress intensity and decreased with thickness according to the energy method. This result is similar to the stress intensity graph from the plate bending approach for a constant defect size to film thickness ratio. This implies that the critical defect size is scaling with film thickness. The critical defect in the thermally grown oxide films are the equiaxed grains produced during growth. Other sources of defects could be from dislocations in the film created from either lattice misfits between the film and substrate, a rough substrate surface, or foreign particles in the substrate. As the film thickness increases and the defects are typically created from the substrate they can become more pronounced.

The fracture pattern is believed to be circumferential around the indentation contact area. Even though the cracking pattern for the thermally grown samples were not able to be directly observed after the first discontinuity, it was shown that at indentations with maximum loads beyond the first discontinuity to have predominately circumferential cracking with crushing of the film beneath the tip's contact area. An anodized aluminum sample was shown to fracture in a circumferential pattern around the indentation. Indentations beyond the first discontinuity of the anodized aluminum showed sequential circumferential cracking of the film.

The approximated stress intensity factors for aluminum oxide thin films on aluminum substrates are in good agreement with observations made by Thurn and Cook. [90] Vapor deposited alumina films were found to have a stress intensity at fracture between 1.7 and 2.1 $MPam^{1/2}$. The stress intensity factor shows that very low loads can cause film fracture with the presence of small surface flaws.

Further development of these methods would require a more intensive investigation into the deformation of the substrate. The atomic structure of materials and crystallographic direction of the loading can have an effect on the deformation. Materials with a face centered cubic crystal structure will deform differently than hexagonal close packed and body centered cubic structures. All three of these crystal structures can form a hard film/soft substrate system through oxidation or by film deposition techniques.

The distribution of the applied load to the film/substrate system is dependent on the tip radius and shape. Indentation tips with a smaller radius produce smaller areas of deformation. This would change the plate approach used to determine the stress intensity at fracture. The energy method should be independent of tip shape. The tip shape could change the fracture pattern and thus change the crack extension force calculation. The numerical results from this study were determined with a single cube corner tip with a radius of 570 nm. However, indentations with a conical tip into an anodized aluminum sample produced similar load-depth curves to the cube corner.

Reference:

[90] J. Thurn and R.F. Cook: Mechanical and thermal properties of physical vapour deposited alumina films: Part II Elastic, plastic, fracture, and adhesive behaviour, *J. Mater. Sci.* **39**, 4809-4819 (2004)